NONLINEARITIES DURING PATTERN FORMATION IN HOLEY METAMATERIALS

A dissertation submitted to the University of Manchester
for the degree of Master of Science
in the Faculty of Science and Engineering

2023

Shresht Jain
Department of Physics and Astronomy

Contents

Word count 7850 words

List of Figures

Abstract

The axial loading of a column is a well known cannonical problem first described by Euler and Bernoulli. Recently, buckling in columns with regular arrays of circular voids was studied experimentally for hard materials, indicating a deviation in post-buckling behaviour from that of elastomeric columns. In this study, we extend the theoretical model of holey columns to incorporate the effects of material nonlinearities. We extend the simplified analytical model proposed by Johnson et. al that considers the column to be a collection of rigid sections connected by a network of thin ligaments acting like fixed torsional springs. Notably, in the updated model, the ligaments are modelled as deformable torsional springs that can undergo compressive and shear deformations. The total energy cost of the deformations is minimised numerically to determine the equilibrium state of the system. The response of the ligaments to deformations was modelled using empirical force-displacement curves of a single ligament under compressive, shearing and rotational deformation. We present results obtained from simulations of the column under axial compression, confirming that material nonlinearities can explain the post-buckling behaviour in hard materials, while retaining the assumption of elasticity. Having established that the compressive response of ligaments in holey columns differs significantly from that of individual ligaments, the compressive response was modelled for the entire column instead of extrapolating from single ligaments. We report that for columns with many holes ($N \geq 11$), such a model can reflect the behaviour observed in experimental investigations with good precision.

Declaration

No portion of the work referred to in the dissertation has been submitted in support of an application for another degree or qualification of this or any other university or other institute of learning.

Intellectual Property Statement

i. The author of this dissertation (including any appendices and/or schedules to this dissertation) owns certain copyright or related rights in it (the "Copyright") and s/he has given The University of Manchester certain rights to use such Copyright, including for administrative purposes.

ii. Copies of this dissertation, either in full or in extracts and whether in hard or electronic copy, may be made **only** in accordance with the Copyright, Designs and Patents Act 1988 (as amended) and regulations issued under it or, where appropriate, in accordance with licensing agreements which the University has entered into. This page must form part of any such copies made.

iii. The ownership of certain Copyright, patents, designs, trade marks and other intellectual property (the "Intellectual Property") and any reproductions of copyright works in the dissertation, for example graphs and tables ("Reproductions"), which may be described in this dissertation, may not be owned by the author and may be owned by third parties. Such Intellectual Property and Reproductions cannot and must not be made available for use without the prior written permission of the owner(s) of the relevant Intellectual Property and/or Reproductions.

iv. Further information on the conditions under which disclosure, publication and commercialisation of this dissertation, the Copyright and any Intellectual Property and/or Reproductions described in it may take place is available in the University IP Policy (see http://documents.manchester.ac.uk/DocuInfo.aspx?DocID=487), in any relevant Dissertation restriction declarations deposited in the University Library, The University Library's regulations (see http://www.manchester.ac.uk/library/aboutus/regulations) and in The University's Guidance on Presentation of Dissertations.

Acknowledgements

I would like to thank Draga for guiding me through out the year, and for her patience and her understanding, in good times and in bad. Chris for being a superb mentor, and teaching me so much about coding and also teaching me how to learn and think. To my Mom, Dad and Sister, who despite an ill timed holiday have been my rock and without whom the good times dont come, and to my many friends whose light warms the day and turns the nights bright.

Chapter 1

Introduction

Buckling of thin columns under axial loading, originally described by Euler and Bernoulli, is one of the textbook problems of modern science: if compression exceeds a critical level, the column does not stay straight but deforms by deforming sideways. The buckling of columns has been a subject of many studies in fields ranging from material sciences [5], biology [6], mechanical and civil engineering [7], to physics and applied mathematics [8]. However, we are only starting to fully characterise the behaviour of columns with an array of regularly spaced holes across their length. For example, when compressed, such columns can stay symmetric with respect to the vertical, because the circular holes transform into an array of vertical and horizontal ellipses that alternate along its length. Most works so far focused on holey columns (and analogous perforated sheets) made out of elastic materials. However, holey columns made of hard materials, such as plastics and metals, also have the same pattern switching behaviour despite deforming plasticly. Post-buckling force-displacement measurements of hard holey columns, however, are qualitatively different compared to that of their elastomeric counterparts, making them ideal for studying the role of coupling between geometrical and material non-linearities in buckling. Exploring this interplay between different sources of non-linearity could find a wide ranging applications, from prosthesis design [9] and soft robotics [10] to automobile design and structural engineering [11].

In this thesis, we will attempt to reproduce experimentally observed post buckling behaviours of hard holey columns and understand them by incorporating non-linear constitutive response of material into a simplified mathematical model. We shall begin

by recapitulating the phenomena of elastic buckling in axially loaded beams. Thereafter, we shall see how this behaviour is linked to pattern switching in columns and sheets with regularly spaced circular holes, and how these structures form an important part of the growing study of auxetics. Finally, we summarise and contextualise the specific phenomena of buckling in holey columns and explore how material nonlinearities may tie into the behaviour of such columns made from hard materials such as metals and plastic.

1.1 Classical Euler-Bernoulli Buckling

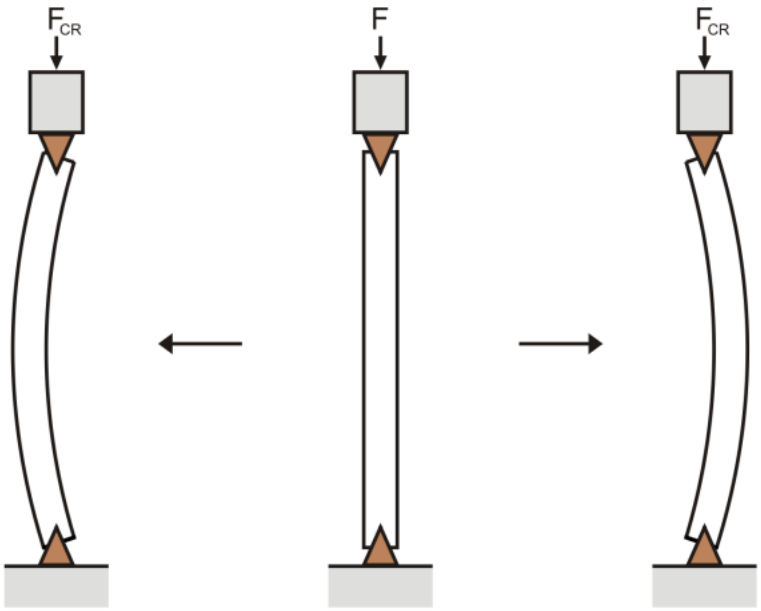

Figure 1.1: An illustration of buckling in an Euler-Bernoulli column under axial compression

Let us start by considering an Euler-Bernoulli column of length L under axial compression given by the force F. As the loading force is increased beyond a critical value given by F_{Cr}, the initial straight state becomes unstable. This critical load is found to be

$$F_{Cr} = \frac{\pi^2 EI}{(kL)^2}, \tag{1.1}$$

where E is the Young's modulus of the material, I is the second moment of inertia of the column and kL defines its effective length (which changes depending on the

particular boundary conditions applied in the problem, e.g. k = 2 for a beam pinned at both top and bottom boundaries) [12]. Upon further increasing the loading force, the left-right symmetry of the system is broken, and the column deforms sideways. This buckling occurs via the pitchfork bifurcation. For a perfect column, there is an equal probability of attaining either the right or the left buckled state, but when imperfect perturbations are applied or if the system contains bias to begin with, an imperfect bifurcation is observed instead and the system preferentially attains one of the two final states [13]. Both scenarios are illustrated in the bifurcation diagrams in Figure 1.2, which can be interpreted as plots of deviation of the column centre from the vertical as a function of the applied force.

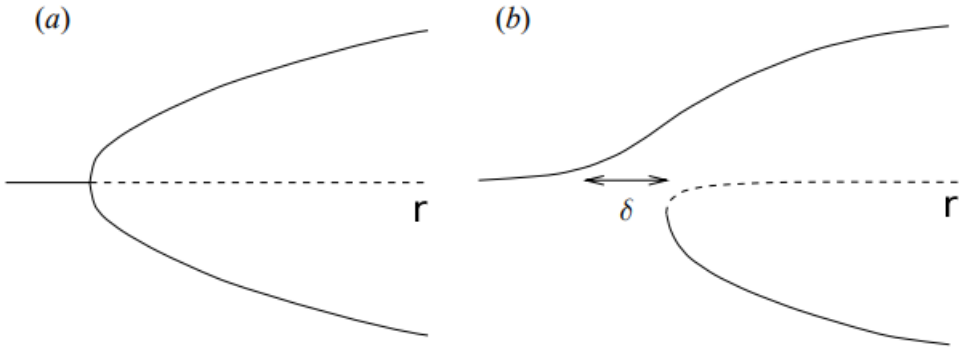

Figure 1.2: a)Perfect and b) Imperfect Pitchfork bifurcations of a system. For our system we can consider the parameter r to be correspond to the Force or displacement that the beam is experiencing [1]

1.2 Buckling Phenomena in Holey Columns

In order to gain an understanding of the phenomena of buckling in holey columns, we hereby recap previous investigations of the system by Pihler-Puzovic et al. [2], Johnson et al [3] and Box et al [4].

A holey column of N holes is obtained by regularly perforating a rectangular Euler-Bernoulli beam along its axis of symmetry. Thus, the D_2 symmetry of the unperforated beam is retained. This corresponds to 3 non-identity operators of symmetry, for which the system is invariant. These are reflections about the horizontal and vertical axes, and rotations of $\frac{\pi}{2}$. However, in contrast to the Euler-Bernoulli beams, the holes in the column introduce an additional symmetry to the system. As all the holes are exactly

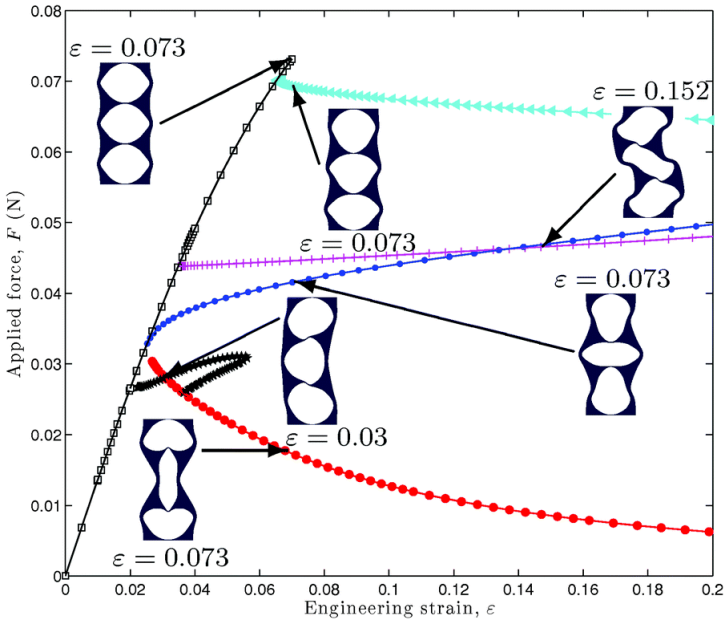

Figure 1.3: Explorations of the various bifurcation modes in a three holed column, using finite element simulations of the column. We can follow the trivial compression branch denoted by the unfilled squares. The 2 alternating mode branches are denoted by circles and are red and blue for vertical and horizontal elipses respectively. We can also observe the Euler branch in black and the mixed modes in pink and cyan respectively[2].

the same, under the assumption that they are perfectly manufactured, we also can exchange any of the holes for each other. Thus, before bifurcation, the system also possesses S_N group symmetry due to the invariance of the system to permutations of the cells. This significantly enriches the bifurcation space [14], as illustrated in Figure 1.3 for the case of columns with 3 holes.

We will refer to the branch of the bifurcation diagram, on which the beam undergoes Hookean compression, without any symmetry breaking, as the trivial compression branch. The two branches that correspond to a breaking of the S_N symmetry will be referred to as alternating modes. For columns with odd numbered holes, such as those illustrated in Figure 1.3, these preserve D_2 symmetry and occur through a transcritical bifurcation. [15] However, for even holed columns, these do not preserve D_2 symmetry and occur through a pitchfork bifurcation. These can occur via the circular holes transforming into alternating ellipses with semi-major axes parallel to horizontal and vertical axes, respectively. For columns with odd numbered holes, we can name the case where the middle hole transforms to an ellipse with a semi-major axis parallel to the horizontal axis of the column, as the horizontal branch. Similarly we can also

define a vertical branch. Finally, the bifurcation corresponding to breaking of the D_2 symmetry while preserving the vertical reflection symmetry corresponds to the lateral buckling of the column and is referred to as the eulerian buckling mode.

1.2.1 Role of Geometries of the Columns

There are three major geometric parameters that define the columns, namely the radius of the holes relative to height of the unit cell, the radius of the hole relative to the width of the unit cell and the number of holes in the column. Upon numerical simulations, it has been shown that the method of buckling the column experiences is determined by the width and height of the column relative to the radius of the holes. For holes that are relatively small as compared to the length and widths of the unit cells, the behaviour of the holey column remains close to that of the Euler-Bernoulli beams. This is because the beams are quite thick due to the small hole sizes, relative to the width and height of the unit cells. Thus, the columns undergo a global eulerian buckling. For other relative widths and heights, we see the dominance of the alternating mode. The parameters and the buckling mode they lead to, can be seen in Figure 1.4.

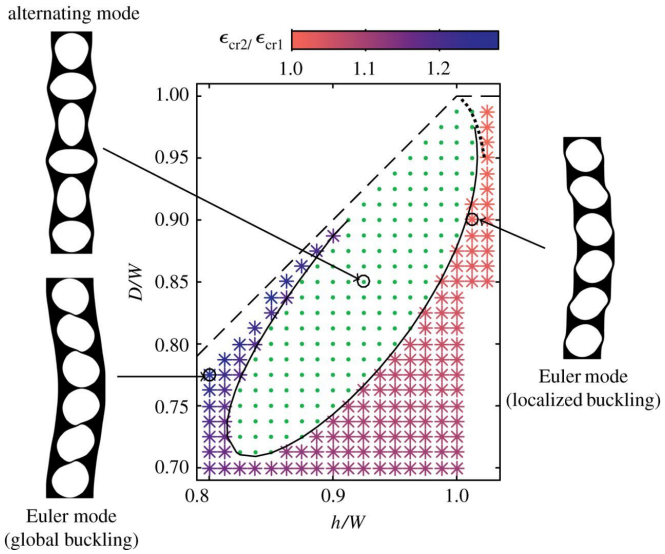

Figure 1.4: Explorations of role of the geometry in the primary buckling mode of a six- holed columns, using finite element simulations of the column. We can observe the dominance of the alternating mode as both the parameters approach 1, which is the asymptotic limit for the radius of the holes and the separation between them approaching the column width[2].

As mentioned in Section 1.2, the parity of the number of holes is crucial to the bifurcation structure of the column, with the alternating mode branch arising through a transcritical bifurcation for odd numbered columns, and pitchfork bifurcation for an even numbered column. However, the critical stress of a column is also affected by the number of holes in the column. the Eulerian buckling mode of the columns scales similarly to the buckling stress of the euler-bernoulli beam, in the limit of columns with a large number of holes. However, for the alternating mode, the critical stress can be expected to tend towards a fixed value as the number of holes increases. The relationship between the critical stress and the number of holes can be seen in Figure 1.5.

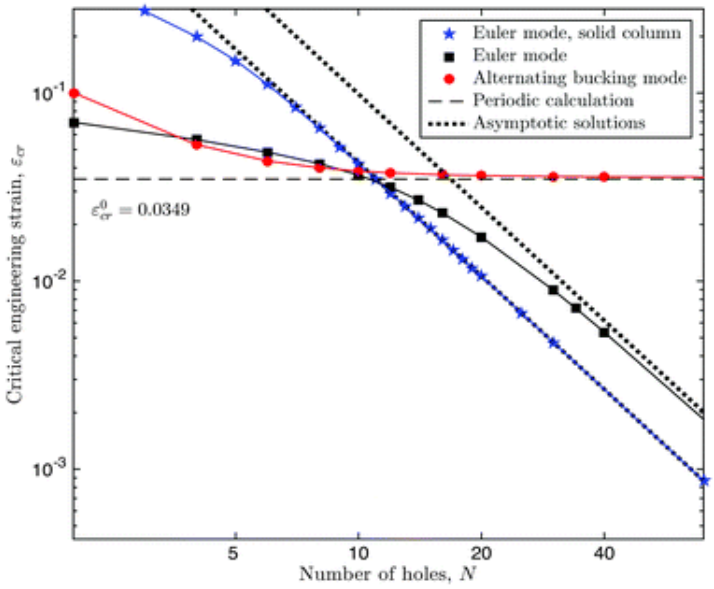

Figure 1.5: Scaling of the critical buckling strain of the various modes of buckling, for increasing number of holes. In the limit of large number of holes, we see the convergence of the alternating mode (red) to a minimal stress of 0.0349, while the Euleriean (black) mode scales as $1/N^2$, which is same as the scaling with increasing length of a solid column undergoing Euleriean buckling. [2].

In finite-element studies of holey columns, it has been previously observed that most of the strain energy of the system is concentrated in the ligaments, labelled w and s in Figure 1.6. It was determined that w and s are much taller than they are thin. These can thus be modelled as euler-bernoulli beams, for thinking of Euler buckling modes in the beams. Additionally, Johnson et al. suggested a simplified model for the holey columns in alternating buckling mode, where the ligaments can be modelled as torsional springs. These were studied theoretically and for the asymptotic limit of

a_s,a_w«D, and the relation between the critical stress for each mode and the parameters a_s and a_w were determined theoretically using the simplified models of the beams.

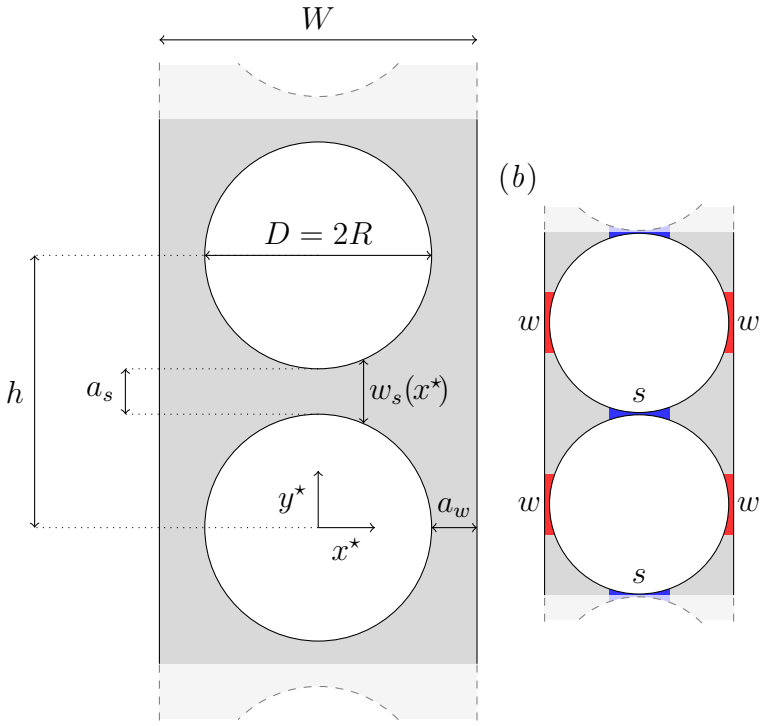

Figure 1.6: An illustration of the geometry of the system used by Johnson et. al[3]. The diameter of the holes are defined as D, the separation between the holes is defined as h, while the width of the column is W. Sub-figure (b) shows the limit of the D approaching W and h approaching D. The thin sections of the column can thus be thought of as Euler-Bernoulli beams labelled s and w. These have widths a_s and a_w respectively, which are also the minimum separation between the holes and column edges.

For beams with elastomeric constitutive behaviour, these models were seen to agree closely to finite element simulations.

1.2.2 Role of the Material of the Columns

The study of these columns has been subsequently extended into columns constructed out of hard materials, as opposed to the elastomeric columns initially studied. It was observed that such columns display significant post-buckling softening behaviour suggesting that the material nonlinearities of harder materials play a significant role in the post buckling behaviour of these columns.

This is the primary motivation for our investigations of the columns. We shall attempt to extend the analytical model of the beam as a torsional, compressive and

shearing spring by incorporating the nonlinear behaviour of these springs into the behaviour of the entire columns. We shall also study the effect that noisy perturbations of the geometry have on these columns, and discuss the results yielded by our investigation.

Chapter 2

Methodology and Model Description

2.1 Model Description

2.1.1 Setting Up the System

As discussed above, Johnson et al proposed a novel, simplified model for modelling the holey columns, where in the alternating mode, the beams can be modelled as a network of torsional springs. However, they assumed that the ligaments could only bend and not otherwise deform. This corresponded to only a single degree of freedom for each rigid piece of the column connected by these ligaments. However, we aim to extend this model by no longer assuming the rigidity of the ligaments. We retain the principle of looking at the rotational deformation of the ligaments as rotation of the rigid pieces that the ligaments connect, as a torsional spring hinge connecting two rigid pieces. However, these ligaments are now deformable and can undergo shearing and compression (or equivalently stretching). However, we consider the ligaments to have some energy cost associated with the deformation and rotation, which are modelled experimentally as we will discuss in Section 2.2. Thus, we extend the model from modelling a two holed column into columns of arbitrary finite lengths characterised as N repeating unit cells of rigid sections connected by a network of springs attatched to deformable hinges. Thus, the energy of the entire system can be thought of as a sum of the individual energy cost associated with the ligaments. To summarise, the columns can be thought of as a collection of rigid mechanisms (also known as T-pieces) that correspond to the thicker portions of the material. These are connected

by a network of the thinner ligaments, which act as springs. These ligaments are resistant to compression, shearing and rotations. This system allows us to model the stress energy of these beams as shown in Figure 2.2.

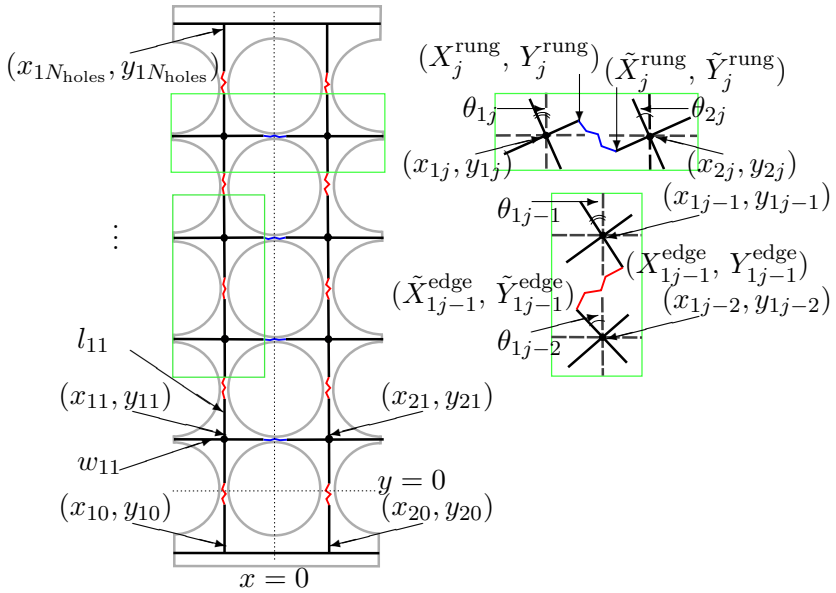

Figure 2.1: The new model of a holey beam with the coordinate system and the rung and edge pieces highlighted. We can define the degrees of freedom of each rigid piece as $\{x_{ij}, y_{ij}, \theta_{ij}\}$. The geometries of these pieces are characterised by their half width (w_{ij}) and the half-length (l_{ij}). Finally we can define $\{X_j^{rung}, Y_j^{rung}\}$ as the coordinates of the left-edge and $\{\tilde{X}_j^{rung}, \tilde{Y}_j^{rung}\}$ as the coordinates of the right-edge of the rung ligaments, respectively. Similarly we can define $\{X_{ij}^{edge}, Y_{ij}^{edge}\}$ and $\{\tilde{X}_{ij}^{edge}, \tilde{Y}_{ij}^{edge}\}$ for the top and bottom edges of the edge ligaments.

We can thus refer to Figure 2.2 in order to define some important terminology. As defined above, T-piece is the name given to the rigid T-shaped parts of the column that are connected by the thin deformable parts of the columns, called ligaments. There are two types of ligaments. The ligaments that are oriented along the horizontal axis are called rungs, as they resemble the rungs of a ladder. The ligaments oriented vertically care called edges as they are located on the edges of our columns. We model the beams as indicated in Figure 2.2, with the origin of our Cartesian coordinate system centered around first pair of ligaments, as seen in Figure 2.1. Thus, each rigid section with half-length (l) and half-width (w) can be characterised by 3 coordinates $\alpha_i = \{x_i, y_i, \theta_i\}$, corresponding to the position of the center of the rigid section in the x and y axis as well as the angular rotation of rigid section defined counterclockwise from the vertical axis. Thus, a beam of N holes can be characterised by $3(2(N-1))$ degrees of freedom corresponding to the x,y and θ coordinates of the $2(N-1)$ T-pieces.

We can also now calculate the total initial length of the column H_0 as

$$H_0 = \sum_{j=0}^{N-1} l_{ij} + \sum_{j=1}^{N} l_{ij}, \text{ for i = 1,2 .} \tag{2.1}$$

where l_{ij} is height of the rigid T-piece i, j where the $i = 1$ corresponds to left half beam and $i = 2$ to the right and j ranges from $j = 0$ and $j = N$ corresponding to the bottom and top pieces of the holey columns. For a holey column with N holes with rigid pieces of uniform lengths, this simplifies to $H_0 = 2N \times l$. Thus, for a beam under $\delta\ell$ compression, the height of the compressed column is given by $H = H_0 - \delta\ell$.
We can determine the equilibrium state of the beam by minimising the energy of the beam after the compression. The energy of the holey column can thus be calculated as the sum of the individual energies of the ligaments. The energy of each ligament depends only on the three degrees of freedom of the 2 T-pieces that are connected by the ligaments. Thus, the energy of the entire holey column is only a function of the degree of freedom vector $\alpha_i = \{x_i, y_i, \theta_i\}$ and thus, at the minima, the following equation is satisfied:

$$\frac{\partial E}{\partial \alpha_i} = 0. \tag{2.2}$$

We shall discuss the problem of minimisation of the energy of the holey columns, subject to the boundary conditions of the column in further detail in Section 2.3.

2.1.2 Finding the Expression for the Energy of the System

As discussed in Section 2.1, the energy of each of the ligaments is a function of its deformation and rotation. The Cartesian coordinate system we initially defined allows us to define the X and Y coordinates of the two ends of the ligaments connecting two rigid T-pieces, which can help us determine their deformation. We can also determine from the system the rotation $\Delta\theta$ of the ligaments. Let us illustrate this in greater detail.

For the horizontal ligaments, we can describe the coordinates of edges of the ligaments as

$$X_j^{rung} = x_{1j} + w_{1j}\cos\theta_{1j}, \quad Y_j^{rung} = y_{1j} + w_{1j}\sin\theta_{1j}, \quad \text{for } 1 \le j \le N_{holes} - 1, \tag{2.3}$$

for the left edge and

$$\tilde{X}_j^{rung} = x_{2j} - w_{2j}\cos\theta_{2j}, \quad \tilde{Y}_j^{rung} = y_{2j} - w_{2j}\sin\theta_{2j}, \quad \text{for } 1 \leq j \leq N_{holes} - 1, \tag{2.4}$$

for the right edge. We can further define the angle rotated by the ligament as

$$\Delta\theta_j^{rung} = \theta_{1j} - \theta_{2j}, \quad \text{for } 1 \leq j \leq N_{holes} - 1. \tag{2.5}$$

The contribution of each of the horizontal ligaments E_j^{rung} to the total energy of the system E^{rung} is some function of the position and rotation of the edges of the ligaments,

$$E^{rung} = \sum_{j}^{N_{holes}-1} E_j^{rung}((X_j - \tilde{X}_j), (Y_j - \tilde{Y}_j), \Delta\theta_j). \tag{2.6}$$

Similarly, for the vertical ligaments, we can define the position and rotation coordinates as follows:

$$X_{ij}^{edge} = x_{ij} + l_{ij}\cos\theta_{ij}, \quad Y_{ij}^{edge} = y_{ij} - l_{ij}\sin\theta_{ij}, \quad \text{for} \quad 1 \leq j \leq N_{holes} - 1,\ i = 1, 2, \tag{2.7}$$

except for the top boundary, which is given by:

$$X_{1N} = -w_{1N}, \quad X_{2N} = w_{2N}, \quad Y_{1,N} = H - l_{1,N} \quad \text{and} \quad Y_{2,N} = H - l_{2,N} \tag{2.8}$$

for the top ends of the ligaments.

Similarly, for the bottom rungs

$$\tilde{X}_{ij}^{edge} = x_{ij-1} - l_{ij-1}\cos\theta_{ij-1}, \quad \tilde{Y}_{ij}^{edge} = y_{ij-1} + l_{ij-1}\sin\theta_{ij-1}, \quad \text{for} \quad 2 \leq j \leq N_{holes},\ i = 1, 2, \tag{2.9}$$

except the bottom boundary, which is given by

$$\tilde{X}_{11} = -w_{11}, \quad \tilde{X}_{21} = w_{21}, \quad \tilde{Y}_{1,1} = 0 \quad \text{and} \quad \tilde{Y}_{1,2} = 0. \tag{2.10}$$

Finally, the rotation of the ligament is given by

$$\Delta\theta_{ij}^{edge} = \theta_{ij} - \theta_{ij-1}, \quad \text{for} \quad 2 \leq j \leq N_{holes-1}, \quad \text{for} \quad i = 1, 2. \tag{2.11}$$

Thus, the total energy of the edge ligaments is given by

$$E^{edge} = \sum_{i=1}^{2}\sum_{j=1}^{N_{holes}} E_{ij}^{edge}((X_{ij} - \tilde{X}_{ij}), (Y_{ij} - \tilde{Y}_{ij}), \theta_{ij}, \theta_{ij-1}), \tag{2.12}$$

where E_{ij}^{edge} is the energy of each of the edge ligaments.

Thus, from equations (2.6) and (2.12), we can now express the energy of the column for a given state of the system, specified by the degree of freedom vector (α_i). However, as the principal axes are fixed for the entire column, we are limited to assuming that the shearing and compression are isotropic for each of the ligaments of the column. This is because for individual T-pieces that are rotated from their original orientation, the shearing and compression deformations of the individual ligaments do not align with the x and y axes that we have defined. In order to generalise the deformation for such ligaments, and to be able to account for anisotropy of the compression and shearing energies, we must transform the coordinate system of the problem into a frame of reference, where the compression deformation of each ligament occurs along one principal axis of the new coordinate system and the shearing along the other. This must be done for all the ligaments in our system. Let us illustrate this for a rung ligament.

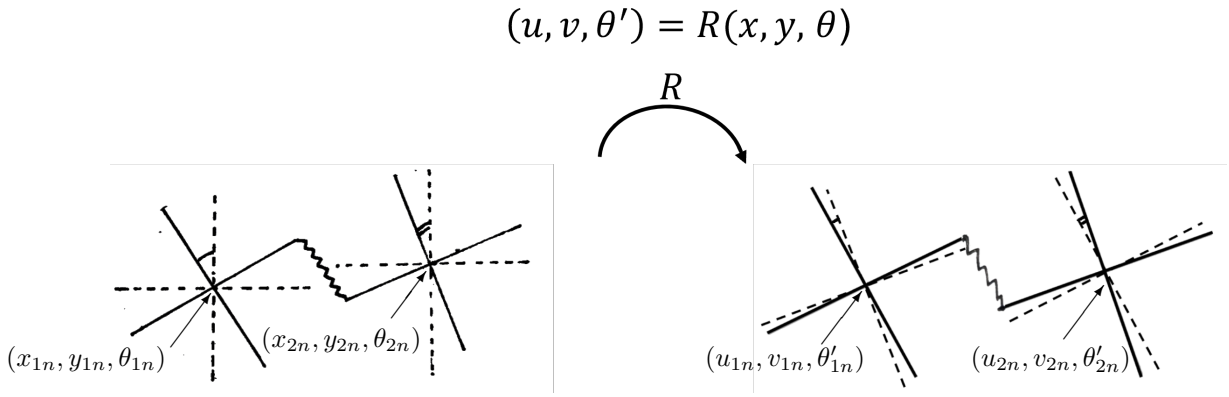

Figure 2.2: Illustration of the old and new coordinate systems and the transformation that allows us to transform between them.

Consider a horizontal ligament connecting 2 rigid pieces, characterised by the 6 degrees of freedom corresponding to the left and right rigid pieces connected by the ligament. These are given by $\{\alpha^l; \alpha^r\} = \{x^l, y^l, \theta^l, x^r, y^r, \theta^r\}$. In order to have the compression and shearing deformations align for this ligament, we can transform the coordinate system under a passive rotation by some angle ϕ. As shown in Figure 2.2, if $\theta^l \neq \theta^r$, in order to align the compressive motion and the shearing motion of the ligaments, we must transform into a coordinate system so that the two angles are

equal. In this new transformed coordinate system, the shearing deformation is along the vertical axis (v) and the compression is along the horizontal axis (u). Thus, we can describe the new coordinate system $\{\beta^l; \beta^r\} = \left\{u^l, v^l, \theta'^l, u^r, v^r, \theta'^r\right\}$.

In order to define the coordinate transformation, we must determine the angle ϕ. Considering two T-pieces rotated through different angles (θ^l) and (θ^r) for the left and right T-pieces respectively. In our new coordinate system, we can see that that the T-pieces will have the same magnitude of the angle they are rotated through denoted by ϑ. Thus,

$$\theta'^l = \theta^l + \phi = |\theta'^r| = \pm(\theta^r + \phi) = \vartheta. \tag{2.13}$$

In the general case (where θ^l may or may not equal θ^r), the positive case ($\theta'^r = \theta^r + \phi$) does not have any non-trivial solutions. Thus, solving for the negative case, we can determine that

$$\phi = -\frac{\theta^l + \theta^r}{2}. \tag{2.14}$$

Thus, we can apply a passive rotation of the principal axes of the T-pieces, $R(-\phi)$ to obtain our new coordinate system. This transformation is given by

$$\begin{aligned}
\theta'^l &= \theta^l + \phi \\
\theta'^r &= \theta^r + \phi \\
u^l &= x^l \cos(-\phi) + y^l \sin(-\phi) \\
u^r &= x^r \cos(-\phi) + y^r \sin(-\phi) \\
v^l &= -x^l \sin(-\phi) + y^l \cos(-\phi) \\
v^r &= -x^r \sin(-\phi) + y^r \cos(-\phi)
\end{aligned} \tag{2.15}$$

Thus, in this new system we can again define the positions of the springs. The positions of the left edge of the ligaments are defined as

$$U_j^{rung} = u_{1j} + w_{1j} \cos\theta'^l, \quad V_j^{rung} = v_{1j} + w_{1j} \sin\theta'^l. \tag{2.16}$$

Thus, we can also define $\{\tilde{U}, \tilde{V}\}$ corresponding to $\{\tilde{X}, \tilde{Y}\}$ as defined in (2.9), defining the new degree of freedom vector $\alpha = \{U, V, \tilde{U}, \tilde{V}, \theta'^l, \theta'^r\}$. This allows us to model the response of the spring to the compression and shearing deformations, as for rung ligaments, all motion in u axis is compressive and in v axis is shear.

Thus, in the rung ligaments, we can model the energy of the ligaments as

$$E^{rung} = \sum_{j=1}^{N_{holes}-1} F^{comp}(U_j - \tilde{U_j}) + G^{shear}(V_j - \tilde{V_j}) + R^{rot}(\Delta\theta). \tag{2.17}$$

Similarly, in our edge ligaments we can see that all the motion in v- axis is compressive while all the motion in u-axis is shear. Thus, we can express the energy of the edge ligaments as

$$E^{edge} = \sum_{i=1}^{2} \sum_{j=1}^{N_{holes}-1} F^{comp}(V_{ij} - \tilde{V_{ij}}) + G^{shear}(U_{ij} - \tilde{U_{ij}}) + R^{rot}(\Delta\theta). \tag{2.18}$$

We can use a variety of nonlinear and linear functions modelled from experimental data to serve as our Compression response function (F^{Comp}), Shearing response function (G^{Shear}) and Rotation response function (R^{rot}). The choice of these functions allows us to model the columns efficiently but effectively and we observe a wide variety of effects as we will discuss in the Section 3. Thus, we can greatly reduce the complexity of the methods we use to model the holey columns, especially as compared to the finite element simulations used previously. However, we still preserve a rich diversity in the behaviour we can model with out technique, depending on our choice of F^{Comp}, G^{Shear} and R^{Rot}. Thus, we use experimental data obtained by Dr. Box to fit for these [16]. Hereafter, we donot continue to make the demarcation that the data was obtained by Dr. Box, but this should be noted.

2.2 Finding the Various Response Functions

2.2.1 Linear Response

Initially, we can begin by assuming a linear behaviour for the response of the springs to the force being applied to them. We can also at this stage make an assumption of isotropic compression, and thus, model the spring compression in both x and y axes by the same constant spring constant k^{disp}. Finally, we can imagine bending to be governed by torsion spring of a spring constant k^{bend}. Thus, we can define the rung energy and edge energies as follows:

$$E^{rung} = \sum_{j=1}^{N_{holes}-1} k^{disp}\left((X_j - \tilde{X}_j)^2 + (Y_j - \tilde{Y}_j)^2\right) + k^{bend}\left(\Delta\theta_j\right) \tag{2.19}$$

$$E^{edge} = \sum_{1=1}^{2} \sum_{j=1}^{N_{holes}-1} k^{disp} \left((X_{ij} - \tilde{X}_{ij})^2 + (Y_{ij} - \tilde{Y}_{ij})^2 \right) + k^{bend} \Delta\theta_{ij} \tag{2.20}$$

and the total energy can be expressed as $E = E^{edge} + E^{rung}$

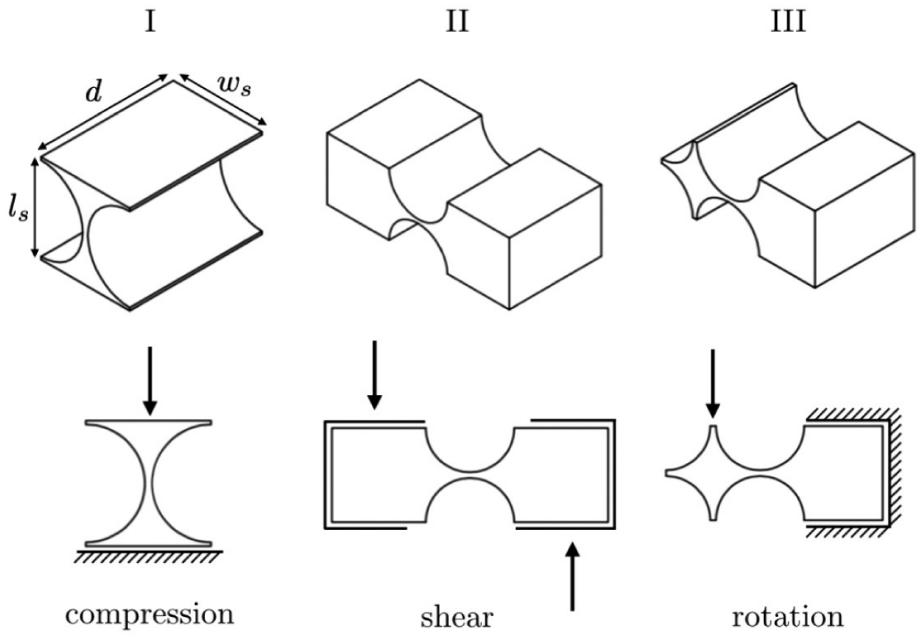

Figure 2.3: An illustration of the experimental techniques employed by Box et al, to gather data for the response of the ligaments to compressive, shear and rotational forces , respectively [4]. Here, the quantities d,w_s and l_s correspond to the thickness, width and length of the individual ligament tested respectively.

In order to determine the response of the springs to compression, shearing and rotation, we use data obtained by Box et al. The data was collected by fabricating 3D printed plastic and milled aluminium ligaments, and subjecting them to compressive, shearing and rotational forces in a Universal Testing System (5569, Instron). The tests for compression, shearing and rotational response of the ligaments were conducted as indicated by Figure 2.3 The typical force and corresponding displacement values from compressing and rotating single ligaments were fitted to a linear function in order to get the the stiffness of the compression and bending of the ligaments.
The values for k^{disp} and k^{bend} obtained were 1005.02 N/mm and 159.12 kJ/rad respectively.

2.2.2 Nonlinear Response for Rotations

In order to capture the non-linearities of the constitutive response of the holey columns under compression, we must take into account the nonlinear response in the single ligaments to rotational torques. Initially the energy of rotation of the springs was modelled as a symmetric function of the form

$$R^{rot}(\Delta\theta) = (a_3|\Delta\theta|^3 + a_2|\Delta\theta|^2) \tag{2.21}$$

. Thus, the torque F corresponding to a rotation through an angle of $\Delta\theta$ is given by

$$F(\Delta\theta) = 3a_3|\Delta\theta|^2 + 2a_2|\Delta\theta| \tag{2.22}$$

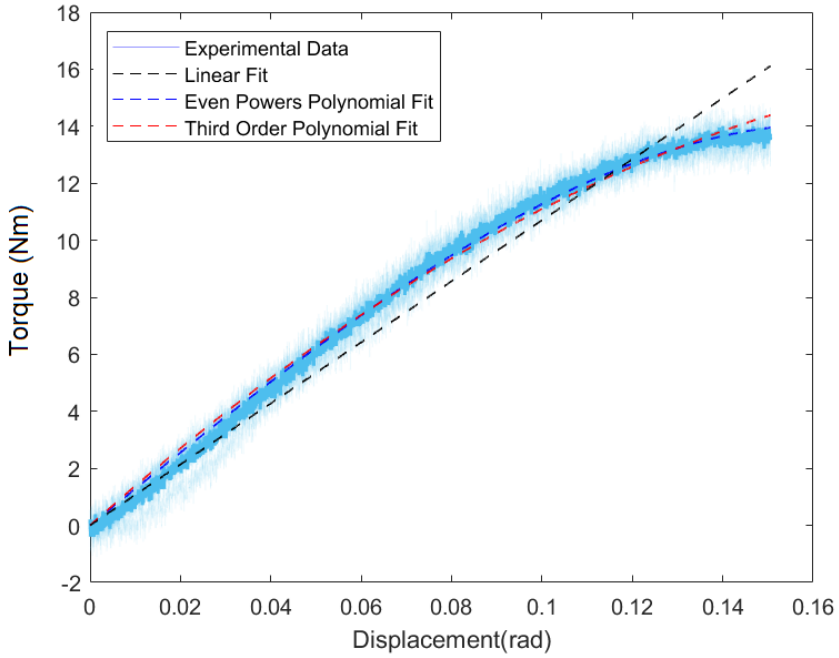

Figure 2.4: Typical values for measured force for the experimental ligament (solid blue) under angular rotation. Indicated alongside are raw measurements (faint blue) from the experiments as well as the linear (dashed black), even power fit (dashed blue) and third order polynomial fit (dashed red) given by (2.19), (2.24) and (2.22), respectively.

Figure 2.4 shows us typical values of force and displacement as determined by the experiments as well as a fit to data for the response given in (2.22). Additionally we have also indicated the fit for the data for response function given by(2.21). The fit values for a_2 and a_3 were determined to be 149.3224 kJ/rad^2 and -101.2284 kJ/rad^3.

However as we will discuss in Section 3, the discontinuity of the modulus function in the constitutive response, has a profound effect on the behaviour of the column. As the modulus function is not continuously differentiable, it produces a sharp 'kink' in the force-displacement curve of the holey columns, as opposed to the smooth function that we would expect. Thus, we can alternatively model the rotational energy as an even polynomial as such a response function would be continuously differentiable. Thus we define

$$R^{rot}(\Delta\theta) = \sum_{i=1}^{n} a_{2n}(\Delta\theta)^{2n} \tag{2.23}$$

. We can choose n in order to incorporate arbitrarily higher order terms, but for the purpose of this study, we will limit ourselves to fourth order polynomials. We can determine the coefficients by fitting the torque to the function

$$F(\Delta\theta) = \sum_{i=1}^{n} 2na_{2n}(\Delta\theta)^{2n-1}. \tag{2.24}$$

We can see from Figure 2.5 that both the functions are suitable fit to our experimental tests, and they are both able to capture the softening behaviour of the ligaments under large rotations.

2.2.3 Nonlinear Response for Compression and Shearing

In order to allow the modelling of holey columns with nonlinear constitutive responses to shearing and compression, we model each individual ligament with an nonlinear constitutive response to the same. To determine this response, as indicated in equation (2.18) and (2.17), we fit the data obtained by tests conducted by Box et al. Figure 2.5A and Figure 2.5B indicate typical values of compression and shearing respectively, as determined by experimental tests described in Section 2. Similar to (2.24), we model the force of compression and shearing as a sum of even powers of the displacement, and the fits are indicated in the Figure 2.5A and Figure 2.5B, respectively. We can see that both these fits appear suitable.

Thus, we can now express the final energy of the column as

$$E^{rung} = \sum_{j=1}^{N_{holes}-1} \left(\sum_{n=1}^{2} a_{2n}(\Delta\theta)^{2n} + \sum_{n=1}^{2} b_{2n}(X_j - \tilde{X}_j)^{2n} + \sum_{n=1}^{2} c_{2n}(Y_j - \tilde{Y}_j)^{2n} \right), \tag{2.25}$$

where a_n, b_n and c_n are the fit parameters corresponding to rotation, compression and shearing respectively. The values for these can be found in Table 1.

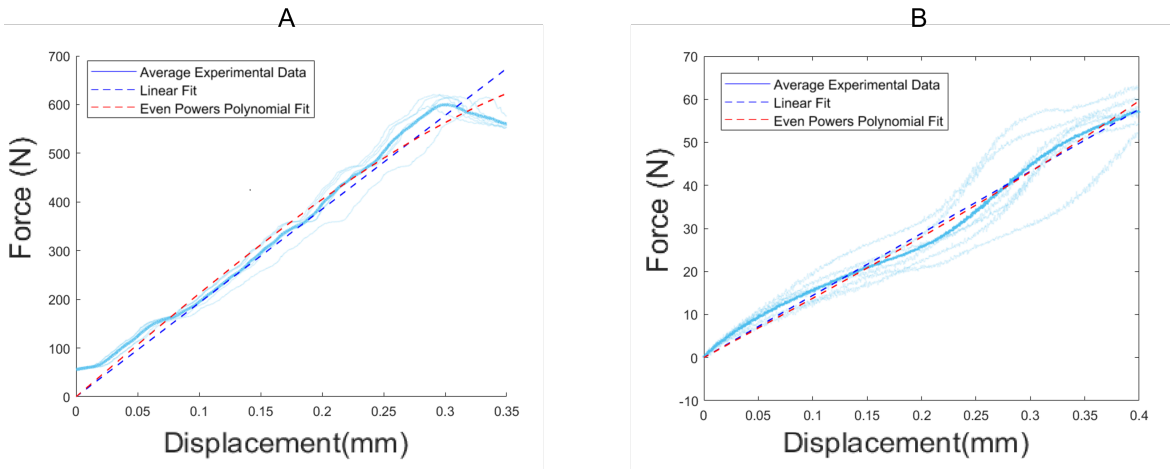

Figure 2.5: (A) Typical values (solid blue) for measured force against compression displacement. Indicated alongside are the raw measurements from experiments (faint blue), as well as linear (dashed blue) and polynomial (dashed red) fits for the data Equation 2.18. (B) Typical values (solid blue) for measured force against shearing displacement. Indicated alongside are the raw measurements from experiments (faint blue), as well as linear (dashed blue) and polynomial (dashed red) fits for the data, as described by 2.18.

Similarly for the edges, we can express the energy as

$$E^{edge} = \sum_{1=1}^{2} \sum_{j=1}^{N_{holes}-1} \left(\sum_{n=1}^{2} a_{2n} \left(\Delta\theta_{ij}\right)^{2n} + \sum_{n=1}^{2} b_{2n} (Y_{ij} - \tilde{Y}_{ij})^{2n} + \sum_{n=1}^{2} c_{2n} (X_{ij} - \tilde{X}_{ij})^{2n} \right). \tag{2.26}$$

We can thus express the total energy as $E = E^{rung} + E^{Edge}$

Parameters of Compression	Fit Value
b_2	1107.11 N/mm
b_4	-1056.07 N/(mm)^3
Parameters of Shearing	Fit Value
c_2	100.50 N/mm
c_4	-641.19 N/(mm)^3
Parameters of Rotation	Fit Value
a_2	159.82 kJ/rad
a_4	-394.88kJ/(rad)^3

Table 2.1: Table of fit parameters as determined by fitting for the compression, shearing and rotation data

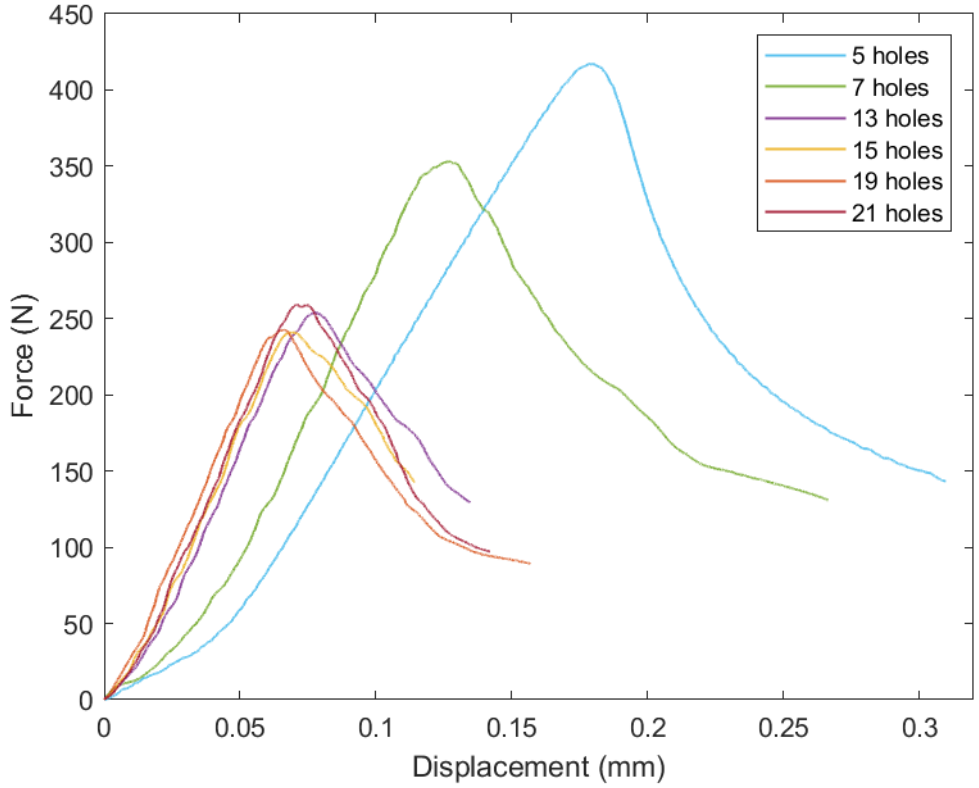

Figure 2.6: Typical values of Force-Displacement per edge ligament of holey columns as determined in experiment. The force-displacement relationship corresponds to Equation (2.27).

2.2.4 Modelling the Compression Response of Entire Columns

Our initial model considers the holey columns as a collection of rigid T-pieces connected by a network of deformable ligaments, where each ligament has an energy cost associated with deforming through compression, shearing and rotation. These energy responses are modelled by collecting experimental data from compression, shearing and rotation of individual ligaments, and fitting their response to the deformations using a polynomial expression, as covered in Section 2.2. However, as we shall see in Section 3, this model falls short of accurately reproducing the experimental behaviour of the holey columns under compression. It was also observed, as covered in Section 2.2, that the main drawback with the model is the difference in behaviour of the individual ligament and the entire column during the initial trivial compression. In order to model the compression response of the entire column, we must determine the force-displacement behaviour of individual ligaments in the holey column. We see that before the pattern switching bifurcation occurs, only the edge ligaments are deformed.

The rung ligaments are merely displaced downwards under compression. Additionally, the edge ligaments also have not undergone any shearing or rotation as the symmetries of the system before bifurcation forbid any shearing or rotation. Thus, we can think of the columns as a collection of ligaments as seen in Figure 2.7. For a N-holed column under some compression x, experiencing some force F, we can consider each parallel collection of edge ligaments to be under $F/2$ effective force. Also, as the individual unit cells must be identical to preserve the S_N symmetry each ligaments must undergo x/N compression. Thus, the new function we must fit to model the compression of the columns is of the form

$$\frac{F}{2} = \sum_{n=1}^{2} b_{2n} (\frac{x}{N})^{2n} \tag{2.27}$$

We scale the data collected from compressing each hole by dividing the compression

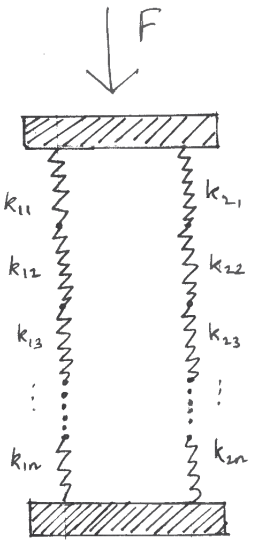

Figure 2.7: Schematic describing the column while on the trivial compression branch. Each ligament deforming under compression is modelled as a spring as indicated.

by the number of holes and the force by 2 respectively. We can see the scaled data in Figure 2.6. Notably, the behaviour of columns with a large number of holes is very similar. We can thus, fit pre-buckling portion of the scaled data in order to find the compression response of each holey column, as seen in Figure 2.7, and thereafter change the compression parameters to reflect the fitted data. The compression response of the holey column is no longer determined by fitting for the compression response of the individual ligaments and extrapolating for the entire network. Instead, we have

decoupled the compression behaviour of the column from the rotation and shearing, and thereafter fit it on a case by case basis for individual holey columns. These new fit parameters are thereafter used to simulate the columns.

Thus, we can summarise the most significant shortcoming of our method thus far as follows: due to significant experimental difficulties in characterising the compression response of the column, we see that the shorter columns suffer from significant contact issues leading to their compression response to differ significantly to longer columns. This is most severe for the individual ligaments, where upon these discrepancies in the responses of the individual ligaments under compression tests and their counterpart being compressed in the entire column cause a significant change in the peak Engineering strain the column can withstand pre-buckling. We worked around this issue by modelling the compression of the individual ligaments from the compression of the entire column (as shown in Figure 2.7), which gives us much better results (as discussed in Chapter 3). However, this comes at the cost of the elegance of being able to model the column entirely by studying only the responses of the individual ligaments and not needing to study the responses of the entire columns, which was the initial idea in our study.

2.3 Solving the System

In order to determine the behaviour of the beam when under compression we must minimise the strain energy inside the column, as indicated by (2.2). In order to do so we first define a degree of freedom vector as follows: $\alpha_i = \{x_i; y_i; \theta_i\}$ and $\beta_j = \{u_j; v_j; \theta'_j\}$ in the original and transformed coordinate systems respectively. Thus, we can define the residual vector as

$$F_i = \frac{\partial E}{\partial \alpha_i}, \tag{2.28}$$

which is zero at the equilibria.

2.3.1 Solving the Eigenvalue problem

The system as formulated by the residual equation (2.28) can be solved numerically by Newton-Raphson, to find for the roots of the residual. Each step of the Newton's

method is defined as

$$x_{n+1} = x_n - \frac{f(x)}{f'(x)} \tag{2.29}$$

In order to implement the NR solver to find the root of the residuals, we must first define the jacobian matrix (J),

$$J_{ij} = \frac{\partial F_i}{\partial \alpha_j} = \frac{\partial^2 E}{\partial \alpha_i \partial \alpha_j} \tag{2.30}$$

. Thus, we can define each step of the NR as

$$\alpha_j^{n+1} = \alpha_j^n - \left(\frac{F_i}{J_{ij}}\right)^n. \tag{2.31}$$

This allows us to solve for the roots of residual function. However, in the symmetric coordinate system, the residuals and the jacobian must be transformed as per the transformation of the coordinate system. Thus,

$$R_i = \frac{\partial E}{\partial \beta_j}\left(\frac{\partial \beta_j}{\partial \alpha_i}\right), \text{ and } J_{ij} = \frac{\partial^2 E}{\partial \beta_k \partial \beta_l}\left(\frac{\partial \beta_k}{\partial \alpha_j}\right)\left(\frac{\partial \beta_l}{\partial \alpha_i}\right) \tag{2.32}$$

The linear stability of a system of ODEs is determined by the sign of the real part of eigenvalues of the Jacobian matrix corresponding to the system. The eigenvalue problem of the Jacobian can be written as

$$J_{ij} e_j^n = \lambda^n e_j^n, \tag{2.33}$$

where e_j^n are the eigenvectors of the Jacobian matrix with a corresponding eigenvalue λ^n. For all eigenmodes e_j^n, if $\Re(\lambda^n) < 0$ then the perturbations of such form are asymptotically stable and will decay. Thus, from if the eigenvalues corresponding to all modes of a particular stationary solution of the system are negative, we can say that the particular stationary state is a stable solution to the problem, and vice versa [17].

In order to encourage the system to break symmetry and undergo a bifurcation, we perturb the system with a perturbation of an amplitude of the eigenvalue (e_j^{max}) corresponding to the maximal eigenvalue (λ^{max}). When this eigenvalue is positive, the equilibrium state is unstable, and perturbations of the form

$$\alpha_j^{n+1} = \alpha_j^n + \varepsilon(e_i) \tag{2.34}$$

allow the system to bifurcate [18]. We can adjust the amplitude of the perturbations (ϵ) in order to explore the bifurcation space of the system.

2.3.2 Solving using the Method of Lagrange Multipliers

The method of solving the residual equation, as described in Section 2.3.1 has two major drawbacks. Firstly, the system can only be controlled by varying the displacement parameter of the system ($\delta\ell$), and solving for the equilibrium state under the updated boundary conditions. The existence of limit points in the displacement parameter continuation of the system makes it so that the system frequently is unable to trace out the entire post bifurcation behaviour of the columns. In order to be able to move around the limit points, a method of doing a parametric continuation in force needs to implemented. Secondly, there is no systematic way of following any particular bifurcation branch of the system and there is a lot of trial and error involved in finding the particular post bifurcation branch. In order to combat both these problems, we adapt the solver to be able to also solve for the equilibrium states of the beams for a given value of force, allowing us to do parametric continuations in both displacement and force.

In order to do so we add two new degrees of freedom to our degrees of freedom vector, corresponding to the force and the height of the column at any given time. Thus, we can solve the minimisation problem for the force by considering a mass of weight equal to the given force pushing down on the column as shown in Figure 2.7. Thus, we must add the contribution of this weight to the energy, corresponding to the potential energy of the weight. Thus, the new energy function of the system (E_{final}) of a system under force (F) for the column height (H) is given by

$$E_{final} = E + (F \times H), \tag{2.35}$$

where E is the energy of the system prior to being loaded by the force. Similarly, the new residual vector has two more terms corresponding to the force applied to the columns and the difference between the current force experienced by the column and the given force. This new energy function is again minimised by finding the roots of the new residual function. Thus, for$R_i = 0$ the force equals the given force as the last term of the residual enforces this while the height of the column corresponds to the height that minimises the energy. This new root finding problem is again solved using the Newton-Raphson method. However in order to solve the problem for a given displacement of the column, we formulate the problem as a Lagrange Multiplier. The

Lagrange function (L) for some function $f(x)$ subject to a constraint $g(x)$ is defined as

$$L(x;\lambda) = f(x) + \lambda g(x) \tag{2.36}$$

, where λ is the unknown Lagrange multiplier. For our system in order to minimise the energy, given the compression of the column as the constraint we can formulate the Lagrange equation as

$$L(\alpha_i) = E(\alpha_i) + F(\alpha_i)(H_g - H), \tag{2.37}$$

where the force (F) is the Lagrange multiplier and H_g is the height of the column subject to the current degrees of freedom and H is the desired column height after δl compression. Thus, we solve the following equations,

$$\frac{\partial L}{\partial \alpha_i} = 0 \text{ and, } \frac{\partial L}{\partial \lambda} = 0. \tag{2.38}$$

These equations are again solved using the method of the Newton-Raphson solver.
Both the aforementioned methods were implemented in MATLAB 2021a and were setup to be able to plot the Engineering Stress-Strain curves as well as investigate the state of the holey columns under force and displacement parameter control.

Chapter 3

Results

3.1 Holey Columns with Linear Elasticity

We start by considering the case of a holey column with 13 holes, for the widths and lengths of the T-pieces defined by $w = l = 4.25$. As indicated in Section 2, we model the column as a network of deformable ligaments. To begin with, we consider these ligaments to have a linear response to all the forms of deformation and rotation. Additionally, we consider the response to deformations along X and Y axes of the ligaments to be isotropic and thus the energy of the system is given by (2.20). The corresponding eigenvalue problem is solved to obtain the force-displacement curves for the column, and these are compared to data obtained by the experimental force-displacement curves obtained for beams with 13 holes in Figure 3.1. These were obtained in tests conducted by another member of our group Dr. Box, as seen in Figure 3.1.

Even in this extremely simplified model, we see that the initial trivial branch of compression and the subsequent post-bifurcation alternating branch are seen in the system. Two representative shapes of the column before and after bifurcation are shown in Figure 3.2 corresponding to points A and B shown in Figure3.1. Thus, at some force, also called the peak force of the column, the column undergoes a pattern transformation and the alternating buckling mode is reached. This phenomenon is also observed qualitatively in the experimental data.

However, the linear model still leaves much to be desired. The peak force of the modelled columns is significantly larger than the peak force measured in experiments.

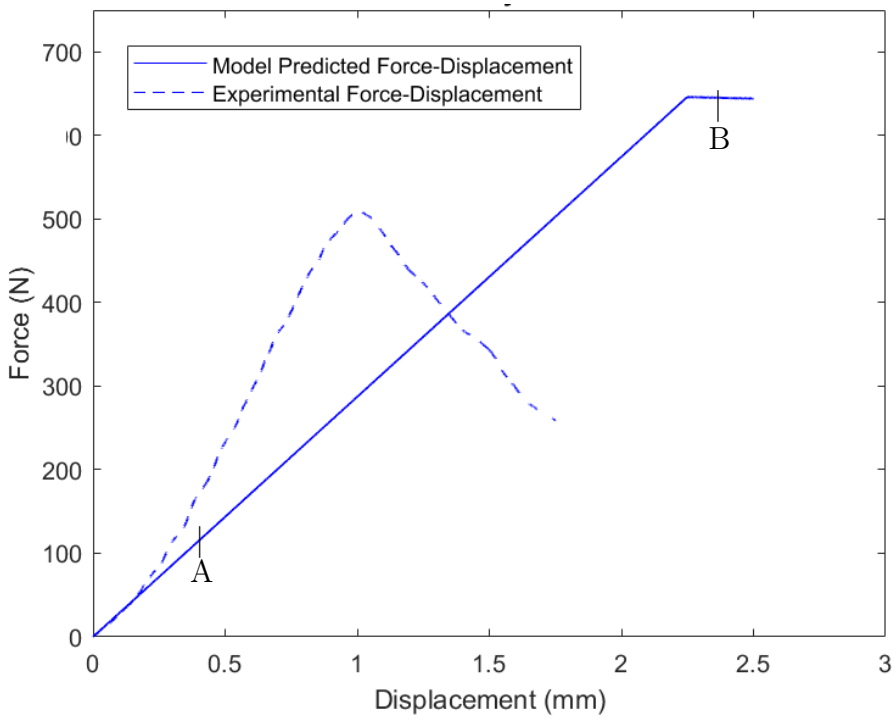

Figure 3.1: Force-Displacement curve for a simulated column with linear constitutive behaviour and experimental data of 13 holes. The state of the column on the initial trivial branch (A) and after pattern formation (B) are labelled.

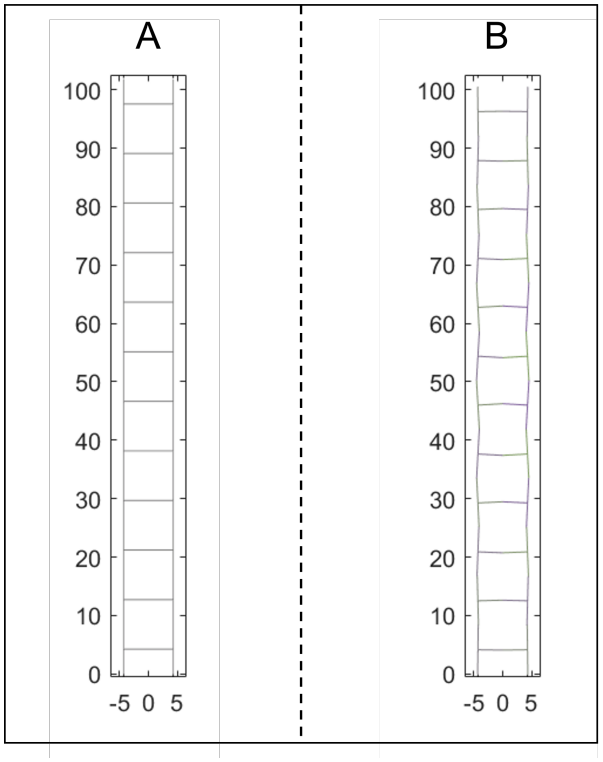

Figure 3.2: State of the column during the trivial compression branch (A) and after the buckling bifurcation (B).

We have also assumed isotropy in the compression of the springs in the x- axis and the y- axis. Consequently, we model the compression in the springs as isotropic to compression and shearing loads, which is an assumption we need to be mindful of going forward. Even more concerning is the fact that the post-buckling behaviour is different from the behaviour measured experimentally. In experimental investigations of hard holey columns, post-buckling softening is observed. Modelling columns that reproduce this softening was an important motivation for our study as discussed in Section 2. In order to reproduce the softening behaviour, we must turn to models of the deformation and rotation of the ligaments with nonlinear constitutive response. On pattern formation, the stress energy of the rotation of the T-pieces becomes very significant, and so we first begin by introducing non-linear rotational response to the system as described in Equation (2.21).

3.2 Adding Nonlinear Rotation to the System

3.2.1 Nonlinearities of the form $a_3|\Delta\theta|^3 + a_2|\Delta\theta|^2$

The rotation energy of the torsion springs must be an even function as the rotation behaviour has to be similar for clockwise and counter-clockwise rotations of the springs. In order to model the rotations of the beam with nonlinear constitutive behaviour we first fit a third order function of the absolute value of the angle rotated, as indicated in (2.21). The force-displacement curve for 13 holed column with such a constitutive response can be seen in Figure 3.3, along with experimentally observed force-displacement for a similar column.

Much like the system with linear response to deformations and rotation, we clearly see the trivial compression as well as the post-buckling branch. The horizontal and vertical branches correspond to the alternating mode buckling occurring parallel or perpendicular to the horizontal axis for the middle (seventh) hole, are also observed, as detailed in Section 1.3. The typical shapes of the column for each of the two, for a column of 11 holes can be seen in Figure 3.4. The symmetry breaking of the S_N permutation symmetry , which characterises the alternating mode of buckling occurs via a trans-critical bifurcation at the critical stress. Encouragingly we see the

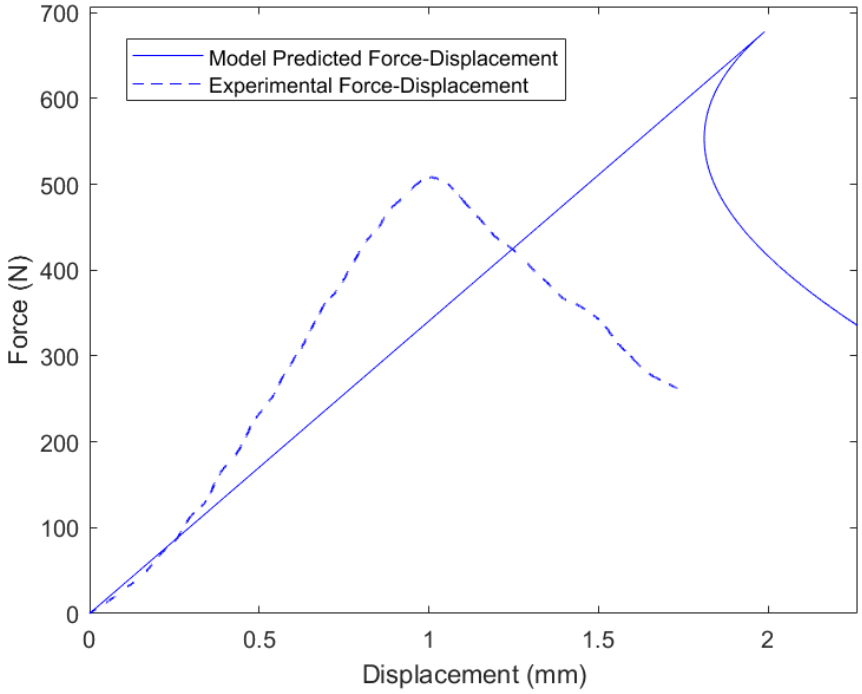

Figure 3.3: Force-Displacement curve for a simulated column (blue solid) and experimental data (blue dashed) of 13 holes. The rotational energy is non-linear and has a constitutive response indicated by (2.21)

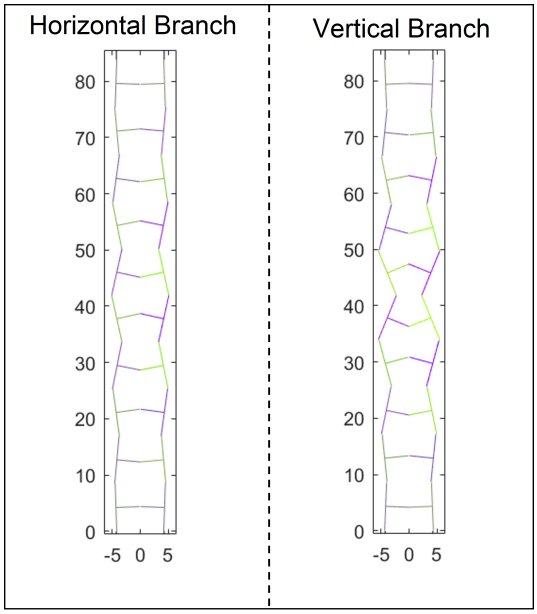

Figure 3.4: State of the column during the horizontal and vertical branches of the bifurcation. We can see the alternating horizontal and vertical deformations and vice-versa. However, under displacement control (which mimic experiments) we only ever observe the horizontal branch and henceforth we only plot this branch.

presence of post buckling softening in the beam, with the system softening rapidly near the bifurcation and exhibiting post buckling softening throughout the bifurcation branch. This clearly is a closer analogue to the behaviour of the columns when studied experimentally. However, there are still two major drawbacks to our model of the system. Firstly, we see that the peak force of the system is extremely high, as compared to experiments, with there being almost a factor of two difference between the simulated and the experimental results. Secondly, the transition from the trivial compression branch to the alternating branches is not smooth, and the force decreases discontinuously on bifurcation. This sharp kink in the curve, is not seen in the experimental beams. It was determined that this behaviour is a consequence of the choice of function chosen to model the constitutive response of the system and close to the bifurcation point, the system behaviour depends on the choice of the constitutive response function chosen to model the energy. The modulus operation of the $|\Delta\theta^3|$ term in the rotational energy of the ligaments is not continuously differentiable near 0. In the case of our chosen function, as described in (2.21), this discontinuous behaviour causes the horizontal and vertical alternating branches to both be located on the same side. Thus, we must seek a constitutive response for the rotation that is continuously differentiable near the point $\Delta\theta = 0$ as well as an even function of $\Delta\theta$. Thereafter, we fit the data to get an expression of the rotational energy as a sum of even powers, as indicated by (2.23) of the angle of rotation, which are always differentiable. We examine the effect this has on the Force-Displacement curve of the system in the next section.

3.2.2 Nonlinearities of the Form $a_4(\Delta\theta)^4 + a_2(\Delta\theta)^2$

As can be seen in Figure 3.3, for simulations of columns with rotational energies as described by (2.23), the typical value of the peak force remains the same as for the constitutive behaviour given by (2.21). However, post-buckling behaviour is significantly different. The simulation of the column with even powers fitted to the rotation energy of the springs allows us to resolve the aforementioned kink in the Force-Displacement curve due to the discontinuity. The bifurcation occurs smoothly, however much like the rotational compression as described in Section 2.3.1, the peak force remains higher than the experimentally observed peak force, by a significant degree. Just like for the

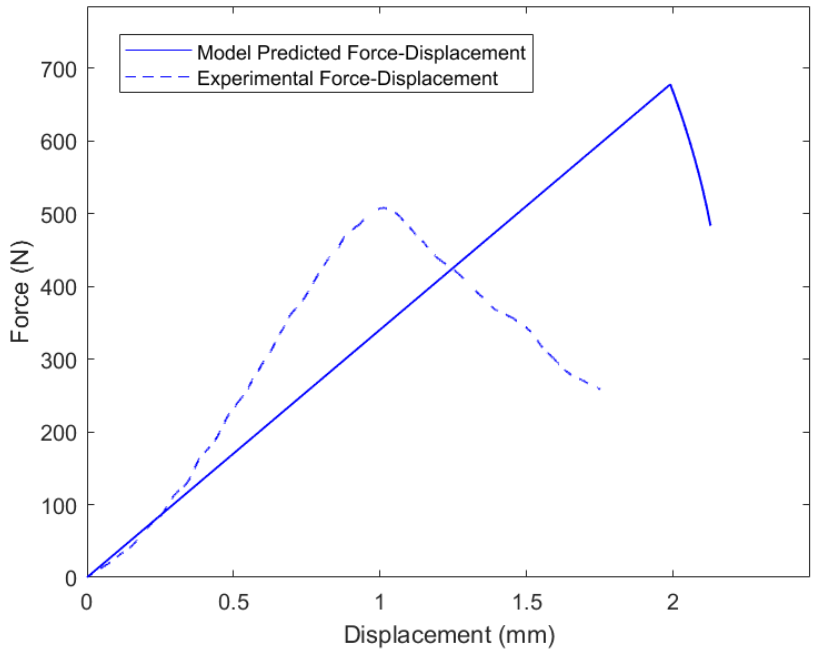

Figure 3.5: The typical values of force and displacement (dashed blue) as recorded experimentally for a 13 holed column using an Instron, along with the simulated behaviour for 13 holed column (solid blue) for the constitutive response defined by (2.23)

previous response, we still have assumed isotropy in the response to compression in X and Y axes. In order to understand the effect of the fit parameters of the rotation response on the column behaviour, we can scale the fitted parameters and then simulate the columns as before.

3.2.3 Effect of a_2 on the Behaviour of the Columns

We investigated the effect of the rotation stiffness on the behaviour of the column, by modelling the beams at varying the first order stiffness of the rotation (a_2) and examining the effect this had on a column of 13 holes. Figure 3.6 shows the force-displacement of the system, for $a_2 = 0, 79.91$ and 159.81 kJ/rad, with a_4 fixed at -394 kJ/rad^3. As we can see in Figure 3.6, the magnitude of a_2 determines the peak stress of the beam, exceeding which the bifurcation occurs and the column falls into the alternating mode buckling state. The less value of a_2, the easier it is for the column to fall into the alternating mode of bifurcation, making the column weaker. Also notably, the post-bifurcation behaviour of the beams does not change with the different values

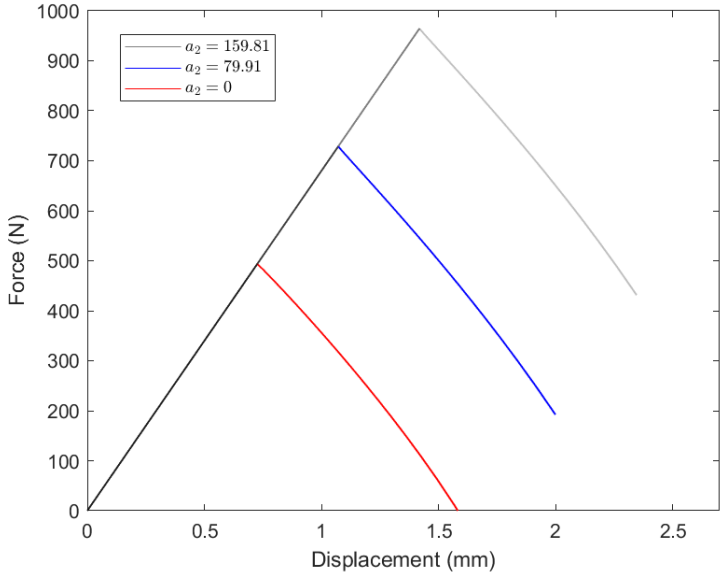

Figure 3.6: Plot of simulated behaviour of a column of 13 holes for $a_2 = 0$ (red) , 79.91 (blue) and 159.81 (grey) kJ/rad, while all other parameters are kept as previously indicated

of a_2 as can be seen from Figure 3.6.

3.2.4 Effect of a_4 on Post Bifurcation Behaviour

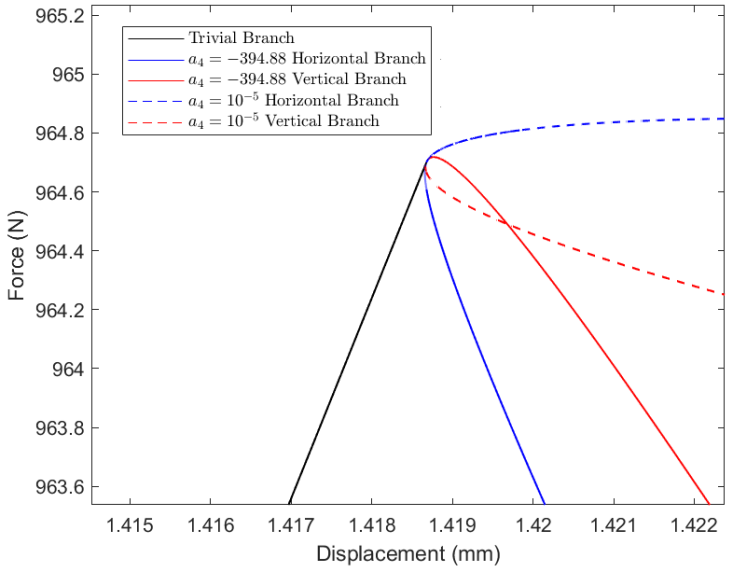

Figure 3.7: Simulated force-displacement curves for $a_4 = 10^{-5}$ (indicated by dashed lines), we see that the horizontal branch (blue) while the vertical branch (red) emerges below. However for $a_4 = -394.88$, (solid lines) it is the opposite. All other parameters are kept as previously indicated

Thereafter, we examine the effect of a_4 on the behaviour of the columns. This is done by fixing a_2, and varying a_4 and simulating the behaviour of the columns. Figure 3.7 shows us the effect of a_4 close to the point of bifurcation. We plot the force-displacement curves for two values of a_4. For $a_4 = 10^{-5}$ (indicated by dashed lines), we see that the horizontal branch (blue) emerges above where the linear case seen in Figure 3.1, while the vertical branch (red) emerges below. However for $a_4 = -394.88$, (solid lines) we see that the order is reversed and the degree of post bifurcation softening is larger for both the branches, as can be indicated by the slope of the branches. see that contrary to the first order bending stiffness, the higher order terms have no effect on the peak stress of the columns. Instead, they greatly influence the post-bifurcation behaviour of the columns.

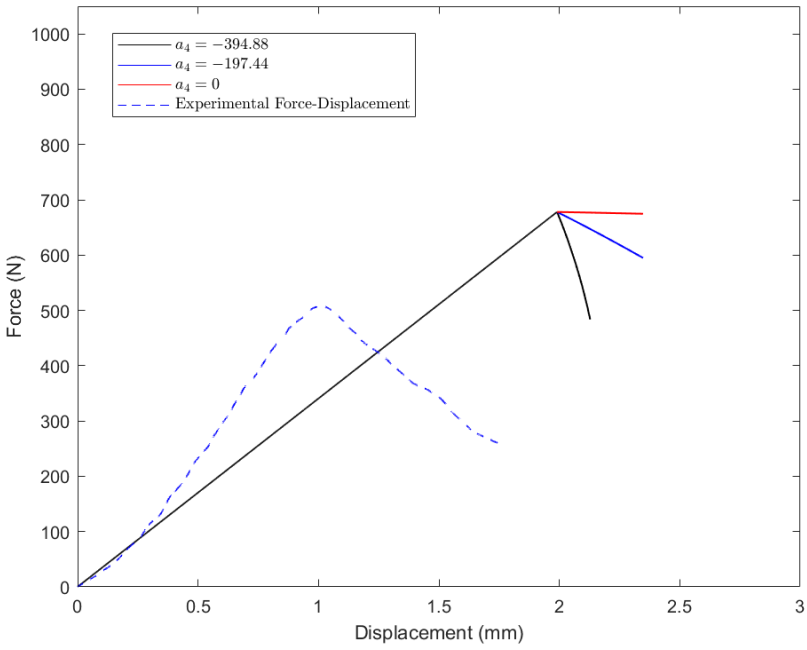

Figure 3.8: Plot of simulated behaviour of a column of 13 holes for $a_4 = 0$ (red) ,197.44(blue) and -394.88 (black) kJ/rad^3, while all other parameters are kept as previously indicated. Also indicated the typical values of force-displacement determined experimentally for a 13 holed columns (dashed blue). Unlike in Figure 3.7, we are only considering the horizontal alternating branches.

We can see that a_4 contributes to greatly to the post-buckling softening behaviour of the column, with its sign and magnitude having an effect of whether the horizontal or the vertical branch occurs at higher force and the degree of post-bifurcation softening respectively. Figure 3.7 and 3.8 allows us to see the effect of the magnitude of a_4

more clearly. In the case of $a_4 = 0$, we recover the behaviour of the linear constitutive response depicted in Figure 3.1. As we increase a_4 to -197.44 and then to the fit value of -394.88 , it is seen that the slope of the bifurcation increases with increasing a_4. Thus, the sign of a_4 determines which of the horizontal or vertical alternating branches shall be at higher force, while the magnitude of a_4 changes the slope of the force-displacement post bifurcation.

However, as the alternating mode of buckling is not just a result of rotation but must also produce some shearing stresses on the T-pieces, we can also further examine the role played by the shearing response of the ligaments and incorporate their effect into the model.

3.3 Adding Constitutive Non-linearity to Shearing Response

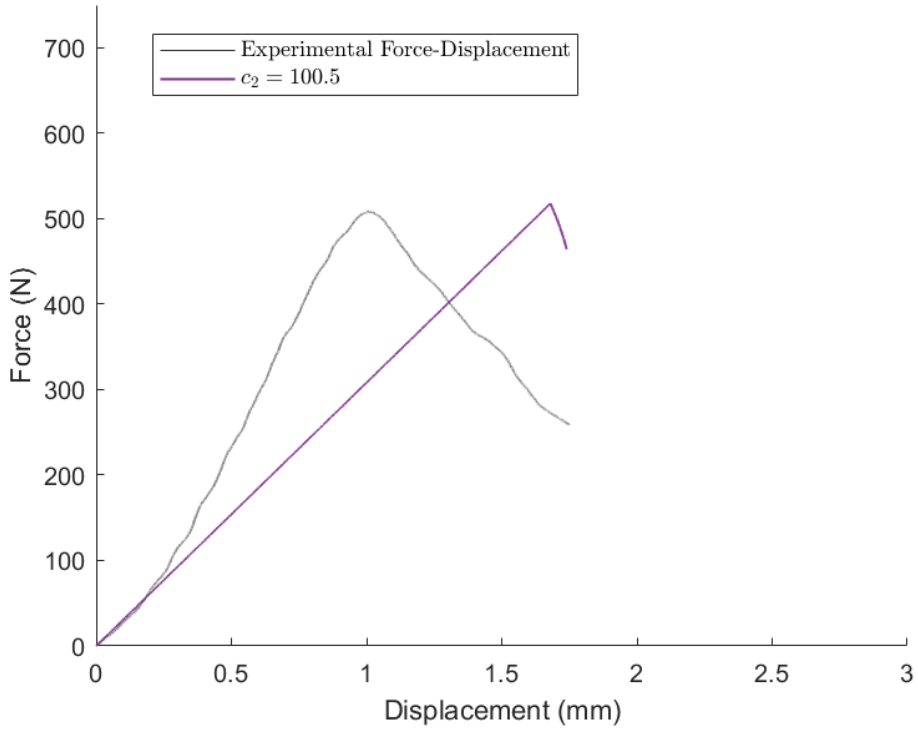

Figure 3.9: Plot of simulated behaviour of a column of 13 holes for $c_2 = 100.50N/mm$, while all other parameters are kept as previously indicated. Also indicated the typical values of force-displacement determined experimentally for a 13 holed columns (grey)

As there still remains a significant gap between the peak stress of the experimental

and the simulated beams, we must now examine assumptions we had made before. Chief among these is the assumption of the isotropic response of the beams to compression and shearing stress. Thus, we now model beams with different response to shearing and compression and furthermore model these beams with nonlinear compression and shearing, as given by (2.18) and (2.17). This is also supported by the results of the fits, as the shearing fit parameters are almost an order of magnitude smaller than the compression, as can be seen in Table 1.

We implemented the nonlinear shearing by implementing the transformed coordinate system and simulating the beams with energy functions as fitted for in Table 1. The resulting force displacement curve as compared to the experimental columns is shown in Figure 3.9.

From the simulations of the nonlinear shearing response, we see, rather encouragingly, that the peak force is within the range of the experimentally measured peak forces. The significant difference between the stiffness of the shearing stress and the compressive strength seems to have been the underlying reason that the experimental columns were much 'weaker' than the simulated ones. Much like the rotational fit parameters we now examine the effect of c_2 and c_4 on the behaviour of the column.

3.3.1 Effects of c_2 on the Columns

Figure 3.10 shows the force-displacement of the system for varying c_2, while c_4 is kept constant at -641.19N/mm^3. The other fit parameters are all fixed as per Table 1.

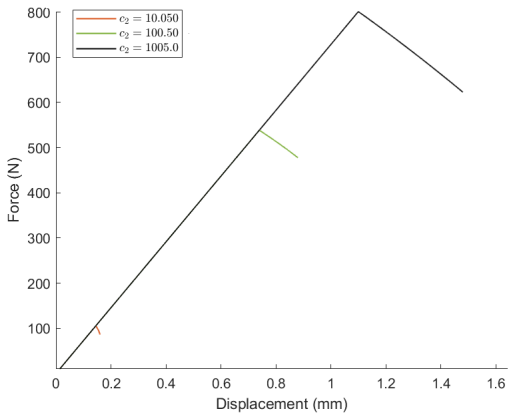

Figure 3.10: Plot of simulated behaviour of a column of 13 holes for $c_2 = 10.050N/mm$ (red), $c_2 = 100.50N/mm$ (green) and $c_2 = 1005.0N/mm$ (black) while all other parameters are kept as previously indicated. Trivial compression branch is marked (black)

We see that just like the parameters of the rotation energy, we see that the c_2 influences the peak force of the column, with lower shear stiffness corresponding to lower peak stresses. For the case of zero shear stiffness, the column has a peak stress of 0 and buckling occurs immediately. So we model the system at the values of c_2 being 10.050 N/mm, 100.50 N/mm and 1005.0 N/mm . Just like rotations, the post-bifurcation behaviour of the columns, seems largely unaffected by c_2, with only the peak force and the point of bifurcation changing.

3.3.2 Effects of c_4 on Post-Bifurcation Behaviour

Figure 3.11 shows the force-displacement of the system for varying c_4, while c_2 is kept constant at 100.50N/mm. The other fit parameters are all fixed according to Table 1.

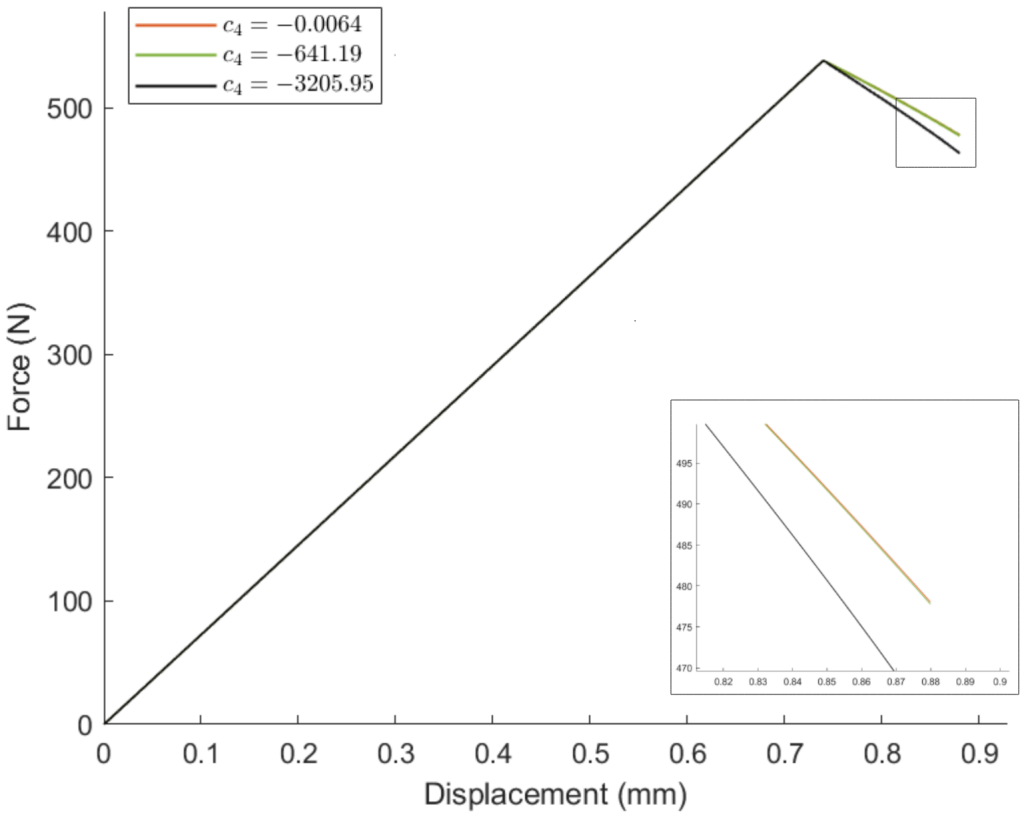

Figure 3.11: Plot of simulated behaviour of a column of 13 holes for $c_4 = -0.0064$ (red), $c_4 = -641.19$ (green) and $c_4 = -3205.95 N/mm^3$ (black) while all other parameters are kept as previously indicated. Trivial compression branch is marked (black)Inset: Zoomed in view of the bifurcation branches to illustrate the weak effect on the beams

From the results of the simulations presented in Figure 3.11, we can conclude

that just like for rotation parameter a_4, c_4 only affects the post bifurcation softening behaviour of the columns and not the bifurcation point or peak force of the columns. However, unlike the non-linear terms of the rotational energy, the post-bifurcation slope does not depend as sensitively on the shearing non-linear terms. This is due to the fact that the rotation of the springs in the alternating mode of buckling is much larger as compared to the shearing displacements of the springs.

3.4 Modelling the Compression Response

Finally we incorporate the fit parameters from the compression data and implement the nonlinear compression in the simulation, as given by the equation (2.25). The combined effect of the non-linear compression, rotation and shearing, with their parameters as indicated in Table 1, can be seen in Figure 3.12.

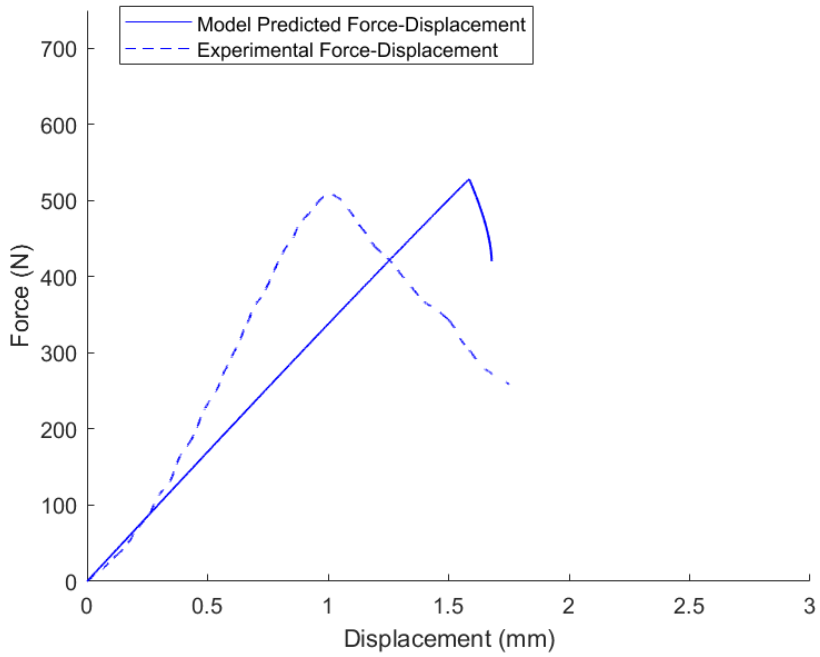

Figure 3.12: Force-Displacement curve of the beam with nonlinear compression, shearing and rotational responses as given by Table 1. Note the peak stress of the beams as well as the close resemblance in the post bifurcation behaviour.

We can see that the peak stress of this column is very close to our experimental data. The post bifurcation behaviour of the beams closely resembles experimentally determined behaviour. However, the displacement that the bifurcation occurs at is very different between the experimental and modelled columns. The difference arises

from the compression stiffening effect that is clearly seen in experimental investigations of the columns as seen in Figure 3.12, while the individual ligaments (Figure 2.5 A) do not display the same. Thus, by incorporating the rotational and shearing nonlinear response, we have successfully managed to model the peak stiffness of the 13-holed column as well as capture the post bifurcation slope of the experimental data. However, the compression response of the beam in the trivial branch is not adequately captured by the model. Clearly, the stiffening effect of the compression in the trivial branch is not accounted for in individual springs. The most likely explanation of this difference in behaviour is variation in the experimental setup of the two systems as well as contact issues in the experiments for the individual springs. In order to better model these beams we no longer extrapolate the compression response of the ligaments in the holey columns from the measured compression response of the single ligaments. Instead this is done individually for each holey column from data collected during axial compression tests.

3.5 Fitting Nonlinear Compression for Entire Columns

As discussed in section 2.4, the nonlinear model of the compression response of individual ligament is insufficient to capture the compression stiffening behaviour of the ligaments of the column in the trivial branch. The behaviour of the entire column appears to be much more nonlinear than the behaviour of an individual ligament under compression. In order to account for this we fit the compression response for each holey column and as described in Section 2.4.1 use this to model the ligaments in the holey columns

A comparison between the compression of fit parameters that were obtained for the case of 7, 13 and 19 holed columns are described in Table 3.1

Thus, in comparison to the fit parameters for a single column, we clearly see that while b_2 for the columns is close to the individual springs, the b_4 terms is an order larger, which would explained by the stiffening effect seen in the columns. However,

Thus, we see that this model improves our ability to model the longer columns like those with 13 or 21 holes. However, for the 7 hole column, there is still a difference in the experimental data obtained and the modelled behaviour. Encouragingly however,

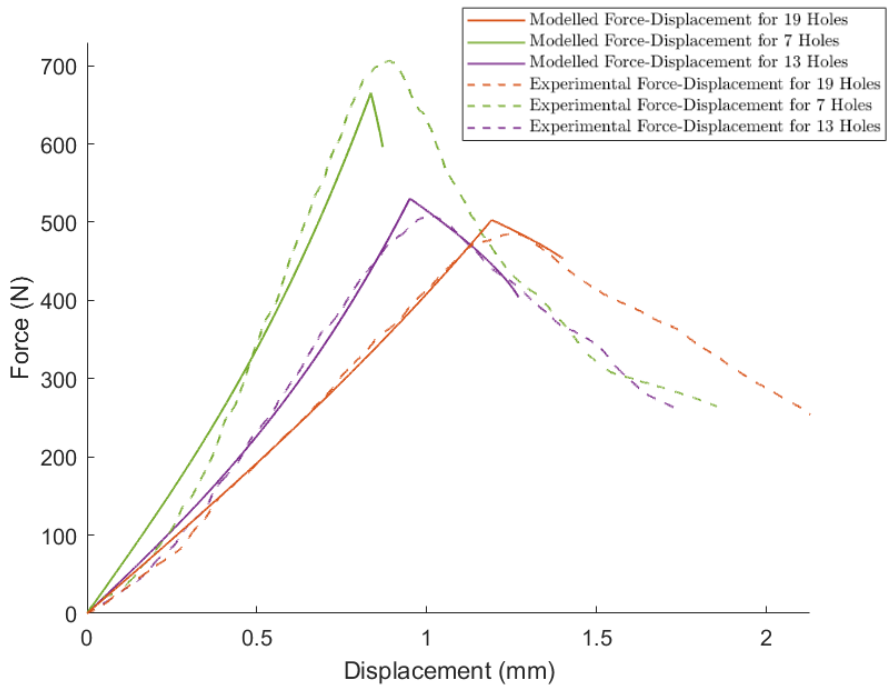

Figure 3.13: Simulated behaviour (solid) compared to typical experimental behaviour (dashed) for beams of 7 (green), 13 (purple) and 19 (orange) holes. The constitutive response to shear and rotation is as indicated by parameters in Table 1, while compression is as indicated in Table 2

Number of Holes	Fit Parameters	
	b_2	b_4
7	1068.91 N/mm	11446.72 N/mm^3
13	1344.77 N/mm	44055.48 N/mm^3
19	1787.68 N/mm	27835.89 N/mm^3

Table 3.1: The values of b_2 and b_4 ascertained by fitting the force-displacement curves of holey columns before they buckle as outlined in (2.27). The rest of the parameters are kept fixed as per Table 2.1.

the post bifurcation behaviour is quite close to the real columns and we have gained an understanding into the effect that these constitutive non-linearities have on the buckling of these holey columns.

3.6 Effect of Perturbations to the Columns

In order to examine the effect of geometric perturbations on the behaviour of the beams, we perturb the half-widths (w_{ij}) and half-lengths (l_{ij}) by some randomly chosen factor ρ. ρ is generated by using a random number generator built into MATLAB to

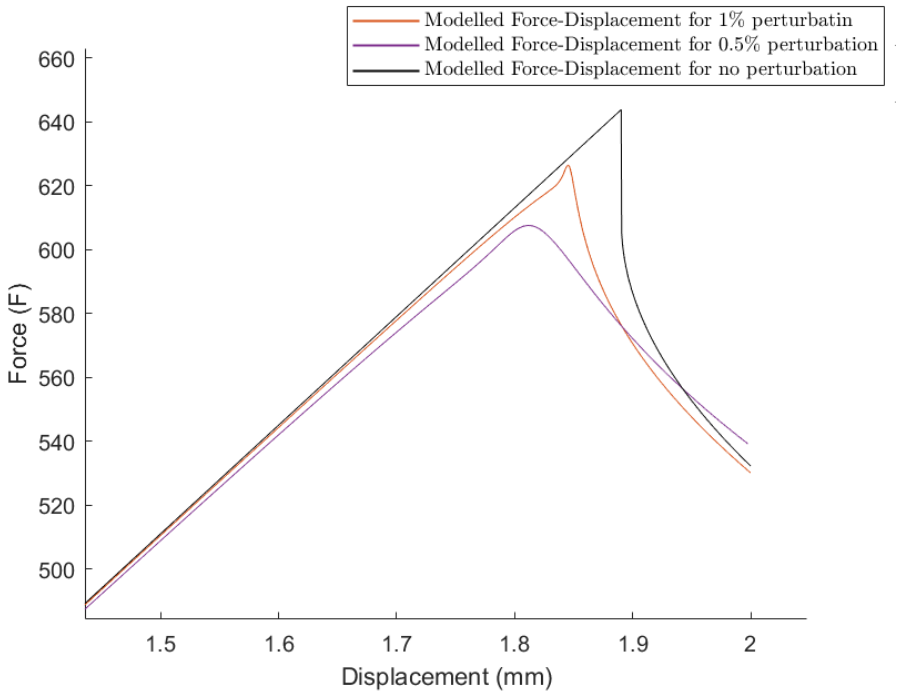

Figure 3.14: Force-displacement curves produced by simulating 13 holed beams for amplitude of geometric perturbation (ε) = 0 (black), 0.005(orange) and 0.01(purple). The other parameters are as described in Section 3.2.1

generate a number from -1 to 1 with a uniform probability distribution. However, these are scaled through some scaling amplitude ε . Thus, the resultant widths are given by $w'_{ij} = w_{ij} + \varepsilon\rho$, and similarly for the lengths. We look at the behaviour of the beams for varying values of the scaling amplitude and these are plotted in Figure 3.14.

Figure 3.14 shows the simulated behaviour of a holey column of 13 holes, when the amplitude is set to 0 (black), 0.5% (orange) and 1% (purple). The constitutive response of the beams chosen for these was the same as the one used in Section 3.2.1. Thus, we still maintain linear compression of stiffness k_disp and assume that the displacements are isotropic along the X and Y axes. It was observed that when the perturbations are applied to the columns, the sharp kink in the Force-Displacement curve gets smoothed out.The peak stress also decreases thus reduces the discrepancy between the experimental holey columns. Also, interestingly sometimes the beams undergo a stress hardening before they undergo the bifurcation and subsequent softening. This deserves further investigation, as we do not yet understand the cause of this effect.

Chapter 4

Discussion

Continuing from work done by Johnson et. al [3] and Box et. al [4], we suggested a novel model for holey columns, in order to simulate the role of material nonlinearities in hard holey columns. We proposed modelling the columns as rigid sections connected by a network of thin ligaments that can deform through compression, shearing and rotation. By minimising the energy of the system, we determined the equilibrium state of the column under compression. Since the outset, there were two major aims of the investigation. Firstly, we aimed to recreate the buckling behaviour and the post buckling softening behaviour seen in the holey columns. Secondly, we wanted the peak force of our simulation to be close to the peak force experimentally determined in our tests. The constitutive response of the ligaments to rotation, shearing and compression was modelled by fitting a polynomial to experimental data collected using an Instron. The constitutive response of the single ligaments to compression, shearing and rotation was then extrapolated to all the ligaments in the network and the behaviour of the column was simulated. We examined the effects of the different parameters of the polynomial fit on the behaviour of the columns. We observed that this extrapolated model was not indicative of the behaviour of columns in experimental investigations. The post-buckling behaviour and peak force of our simulated columns were close to the experimental observations for columns whose compression was extrapolated from tests conducted on single ligaments. However, the compression associated with the bifurcation was not and the model could not accurately reflect the behaviour of the experimental columns. Thus, the compression response of the ligaments in the holey column were modelled using the force-compression behaviour of the entire column

while under compression. With this technique, our simulations are accurately able to reflect the bifurcation point, peak force as well as post bifurcation behaviour of the hard holey column, especially for longer columns ($N \geq 11$). However, these improvements are made at the cost of no longer having the generality of the previous model. Finally the weakening effects of geometric perturbations on the system was presented. Despite best effort to provide a comprehensive and accurate picture of behaviour of hard holey columns before and after buckling, there are many untied threads and open questions. During experiments, it was observed that the pattern transformation needed for the materials to buckle were compression rate dependant. However, as the model is quasi-steady, we have been unable to gain any insight into explaining this very unusual phenomena with our model. Moreover, the inability of the compressive behaviour of predicted by the network single ligaments to accurately reflect that of entire columns collected remains a mystery. We suspect it may be cause by systematic issues in the experimental technique employed while collecting the compressive data of springs, though more exotic phenomena may also be causing it. However many refinements to the experimental method must be made before we can hazard an explanation for this discrepancy . Other interesting avenues of research to continue this line of investigation would be to extend the model to 2D sheets from 1D columns. Finally, while we added small random perturbations to geometry of the system, there is reason to investigate the effect of perturbing the geometry of specific units, as such techniques have previously been applied to create tunable and programmable materials.

Bibliography

[1] A. Juel, A. Darbyshire, T. Mullin, and A. G. Darbyshire, "The effect of noise on pitchfork and hopf bifurcations," 1997.

[2] D. Pihler-PuzoviÄ, A. L. Hazel, and T. Mullin, "Buckling of a holey column," *Soft Matter*, vol. 12, pp. 7112–7118, 2016.

[3] C. G. Johnson, U. Jain, A. L. Hazel, D. Pihler-puzovic, and T. Mullin, "On the buckling of an elastic holey column," vol. 473, Royal Society Publishing, 11 2017.

[4] F. Box, C. G. Johnson, and D. Pihler-PuzoviÄ, "Hard auxetic metamaterials," *Extreme Mechanics Letters*, vol. 40, p. 100980, 10 2020.

[5] X.-L. Zhao, *Cold-formed tubular members and connections : structural behaviour and design*. Oxford ;: Elsevier, 1st ed. ed., 2005.

[6] B. B. Audoly, *Elasticity and geometry : from hair curls to the non-linear response of shells*. Oxford University Press, 2010.

[7] C. Yuzhen, "Buckling of columns and films: from fundamental mechanics to functional materials," 2021.

[8] S. H. Kang, S. Shan, W. L. Noorduin, M. Khan, J. Aizenberg, and K. Bertoldi, "Buckling-induced reversible symmetry breaking and amplification of chirality using supported cellular structures," *Advanced Materials*, vol. 25, pp. 3380–3385, 6 2013.

[9] Y. Kim, K. H. Son, J. W. Lee, C. . Kim, Y. . Son, and K. H. . Lee, "Auxetic structures for tissue engineering scaffolds and biomedical devices," 2021.

[10] P. Kaarthik, F. L. Sanchez, J. Avtges, and R. L. Truby, "Motorized, untethered soft robots via 3d printed auxetics â ," 2022.

[11] A. Lowe and R. S. Lakes, "Negative poisson's ratio foam as seat cushion material."

[12] E. Carrera and M. Petrolo, *Beam Structures Classical and Advanced Theories*. 2011.

[13] C. Coulais, J. T. Overvelde, L. A. Lubbers, K. Bertoldi, and M. V. Hecke, "Discontinuous buckling of wide beams and metabeams," *Physical Review Letters*, vol. 115, 7 2015.

[14] M. Golubitsky and D. G. Schaeffer, *Singularities and Groups in Bifurcation Theory*. Springer-Verlag, 1985.

[15] G. Gaeta, "Bifurcation and symmetry breaking," *Physics Reports*, vol. 189, pp. 1–87, 5 1990.

[16] F. Box, "Personal communication," 3 2022.

[17] J. K. Hale and H. Koçak, *Dynamics and bifurcations*, vol. 3. Springer Science & Business Media, 2012.

[18] C. Coulais, C. Kettenis, and M. van Hecke, "A characteristic length scale causes anomalous size effects and boundary programmability in mechanical metamaterials," *Nature Physics*, vol. 14, no. 1, pp. 40–44, 2018.